



HAL
open science

Optimization of ^{186}Os / ^{188}Os analyses by N-TIMS using amplifiers equipped with 10 13 Ohm resistors

Laurie Reisberg, Catherine Zimmermann

► To cite this version:

Laurie Reisberg, Catherine Zimmermann. Optimization of ^{186}Os / ^{188}Os analyses by N-TIMS using amplifiers equipped with 10 13 Ohm resistors. *Geostandards and Geoanalytical Research*, 2021, 45 (2), pp.287-311. 10.1111/ggr.12371 . hal-03325882

HAL Id: hal-03325882

<https://hal.univ-lorraine.fr/hal-03325882>

Submitted on 25 Aug 2021

HAL is a multi-disciplinary open access archive for the deposit and dissemination of scientific research documents, whether they are published or not. The documents may come from teaching and research institutions in France or abroad, or from public or private research centers.

L'archive ouverte pluridisciplinaire **HAL**, est destinée au dépôt et à la diffusion de documents scientifiques de niveau recherche, publiés ou non, émanant des établissements d'enseignement et de recherche français ou étrangers, des laboratoires publics ou privés.

Optimization of $^{186}\text{Os}/^{188}\text{Os}$ analyses by N-TIMS using amplifiers equipped with 10^{13} Ohm resistors

Laurie Reisberg^{1*}

Catherine Zimmermann¹

¹ Centre de Recherches Pétrographiques et Géochimiques

UMR 7358 CNRS - Université de Lorraine

15 rue Notre Dame des Pauvres

54501 Vandoeuvre-les-Nancy, FRANCE

*corresponding author. email: laurie.reisberg@univ-lorraine.fr

+33 383 594249

Abstract

Analysis of $^{186}\text{Os}/^{188}\text{Os}$ variations in most natural samples is hampered by their low Os concentrations (usually <100 pg/g), requiring Os separation from up to a kilogram of powder to obtain high precision results. Recently developed amplifiers equipped with 10^{13} Ohm feedback resistors improve the signal to noise ratio by an order of magnitude, allowing acquisition of high precision data (2SE <50 ppm) from $^{186}\text{OsO}_3^-$ ion beams of ~ 40 fA, and thus analysis of less material (~ 10 to 500g). Factors controlling the accuracy and precision of $^{186}\text{Os}/^{188}\text{Os}$ NTIMS analyses, using a mixed array of 10^{13} and 10^{11} Ohm amplifiers, include isobaric interferences, baseline variability, gain calibration, decay time corrections and oxygen isotope composition variations. Isobaric interferences present the greatest challenges, but these can be largely overcome by using double Pt filaments and periodically monitoring interferences during each analysis. The optimized procedures produce $^{186}\text{Os}/^{188}\text{Os}$ ratios with precisions close to the theoretical limits imposed by counting statistics and Johnson-Nyquist electronic noise for ion beams of 10 to 70 fA. The long term reproducibility (85 ppm; 2σ) approaches theoretically expected values (~ 50 to 80 ppm). This reproducibility is sufficient to allow $^{186}\text{Os}/^{188}\text{Os}$ analyses of crustal rocks, for which relatively large variations are expected.

Keywords: Os isotopes, ^{186}Os , 10^{13} Ohm amplifiers

Introduction

Osmium has two isotopes of partly radiogenic origin, ^{187}Os and ^{186}Os , formed respectively by the radioactive decay of ^{187}Re and ^{190}Pt . While studies of $^{187}\text{Os}/^{188}\text{Os}$ variations in geological samples have become commonplace, analyses of $^{186}\text{Os}/^{188}\text{Os}$ remain rare. This is because the range of variation of $^{186}\text{Os}/^{188}\text{Os}$ is quite limited in most common sample types (e.g. <0.000020 in young mantle samples (Brandon et al., 1999)), both because of the exceedingly long half-life of ^{190}Pt (4.5×10^{11} yr; $\lambda = 1.48 \times 10^{-12}$ yr $^{-1}$; (Walker et al., 1997)), about ten times greater than that of ^{187}Re , and because of the very low isotopic abundance of ^{190}Pt (0.014%). As a result, high precision analyses are needed to distinguish natural variations of ^{186}Os abundances. This difficulty is compounded by the extremely low Os contents of most terrestrial samples. For this reason, studies of $^{186}\text{Os}/^{188}\text{Os}$ variations have been mostly limited to materials with relatively high Os concentrations (several hundred ppt to several ppb). Examples include extraterrestrial samples (Brandon et al., 2006), mantle peridotites (Brandon et al., 2000; Chatterjee and Lassiter, 2016), ultramafic intrusions (Day and O'Driscoll, 2019) and Mg-rich volcanic rocks such as komatiites, picrites and certain ocean island basalts (Brandon et al., 1999; Ireland et al., 2011; Puchtel et al., 2004). Conventional $^{186}\text{Os}/^{188}\text{Os}$ analysis of crustal samples, which typically contain only tens of ppt of Os, requires Os extraction from hundreds of grams of material to obtain high precision results and thus very few such studies have been undertaken, a notable exception being that of McDaniel et al. (2004).

The development of amplifiers equipped with 10^{12} and 10^{13} Ohm resistors in their feedback loops (which will be referred to here as 10^{13} Ohm amplifiers for brevity), instead of the 10^{11} Ohm resistors used traditionally, has opened up the possibility of high precision analyses of smaller quantities of sample material. This is because the signal/noise ratio of the amplifiers, which is the dominant source of uncertainty on small intensity signals, varies with the square root of the amplifier resistance, and so should be reduced by factors of nearly 3.3 and 10 respectively in 10^{12} and 10^{13} Ohm amplifiers relative to 10^{11} Ohm amplifiers. Recently, 10^{12} Ohm amplifiers have been used to measure $^{186}\text{Os}/^{188}\text{Os}$ variations on small to moderate signals with considerable success (Liu and Pearson, 2014). Koornneef et al. (2014) used 10^{13} amplifiers to measure Sr and Nd isotopic variations by thermal ionization mass spectrometry (TIMS) in quantities as low as 10 pg, achieving a reproducibility of 125 ppm on 100 pg loads of Nd. Other TIMS applications for these amplifiers have been developed for Pb isotopes (Klaver et al., 2015), U/Pb zircon dating (Quadt et al., 2016) and U isotopes (Trinquier and Komander, 2016), while MC-ICP-MS applications include Pt isotope analysis (Creech et al., 2020), and in combination with laser ablation, *in situ* analysis of Pb isotopes (Kimura et al., 2016). Recently, Wang et al. (2019) showed that use of 10^{13} Ohm amplifiers allows

precisions of 2-3‰ to be obtained for $^{187}\text{Os}/^{188}\text{Os}$ measurements of several tens of picograms of Os, demonstrating that these detectors equal or exceed the performance of secondary electron multipliers for these sample sizes. For $^{186}\text{Os}/^{188}\text{Os}$ analyses, precision and accuracy better than a few hundred ppm are often required to obtain geologically useful information. Our goal here is to explore the factors that optimize the precision and reproducibility of $^{186}\text{Os}/^{188}\text{Os}$ ratios obtained from low intensity OsO_3^- ion beams measured with 10^{13} Ohm amplifiers.

Advantages and limitations of 10^{13} Ohm amplifiers

Use of 10^{13} Ohm amplifiers increases the signal intensity in V by a factor of 100 relative to traditional 10^{11} Ohm amplifiers. More importantly, it increases the signal to noise ratio by an order of magnitude. The reason for this is evident from the Johnson-Nyquist equation (Johnson, 1928; Nyquist, 1928), which expresses the magnitude in volts of electronic noise caused by thermal agitation in the resistor:

$$V_{JN} = \sqrt{\frac{4 \times k_B \times R \times T}{t}} \quad (1)$$

where k_B is the Boltzmann constant (1.38×10^{-23} J/°K), R is the resistance in Ohms, T is the amplifier temperature in °K, and t is the integration time in seconds. The improvement obtained through use of 10^{13} Ohm rather than 10^{11} Ohm resistors is visually evident in Fig. 1, which compares the signal of $^{186}\text{OsO}_3^-$ (measured with a 10^{13} Ohm amplifier) and $^{187}\text{OsOsO}_3^-$ (measured with a 10^{11} Ohm amplifier).

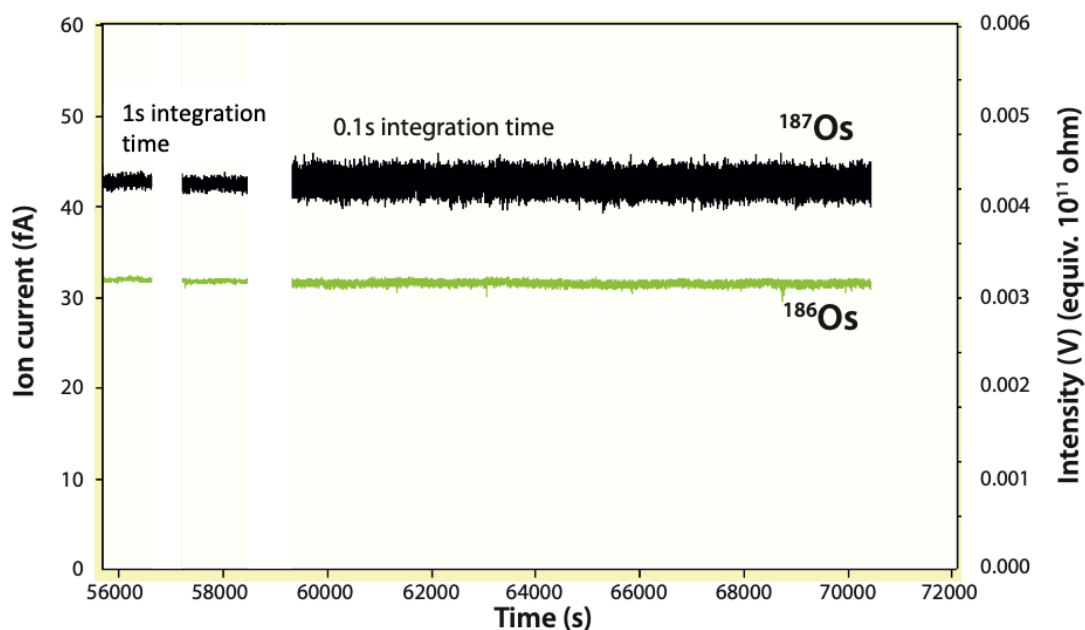


Figure 1. Comparison of signals of $^{186}\text{OsO}_3^-$ ion beam (measured with a 10^{13} Ohm amplifier) with $^{187}\text{OsO}_3^-$ ion beam (measured with a 10^{11} Ohm amplifier) on a DROsS standard, which has comparable isotopic abundances of ^{187}Os and ^{186}Os . To facilitate comparison between amplifiers, signal intensities are presented both as ion currents (fA) and as equivalent volts that would be obtained if the signals were measured with 10^{11} Ohm amplifiers. Gaps in traces represent times when peaks were switched that were erased for clarity.

In addition to directly decreasing the random variability of measured signals, the higher signal/noise ratio provided by the 10^{13} amplifiers improves performance by providing quieter baselines and more reproducible gains for a given calibration current, as will be discussed in detail below.

There are nevertheless two trade-offs for the improved signal/noise ratio of the 10^{13} Ohm amplifiers that must be considered when developing analytical routines. One is that amplifier saturation occurs at much lower signal intensities than for 10^{12} or 10^{11} Ohm amplifiers. In the Triton, saturation of the 10^{13} Ohm amplifiers occurs at ion beam currents of about 1500 fA (0.15 V - here and elsewhere equivalent voltages that would be measured on 10^{11} Ohm amplifiers are given for convenience) in negative ion mode, and about 5000 fA (0.5 V) in positive ion mode, values that are two orders of magnitude lower than those leading to saturation of 10^{11} Ohm amplifiers. This must be taken into account when choosing which isotopes to measure with the 10^{13} Ohm amplifiers. The other limitation is that the time response of the 10^{13} Ohm amplifiers is much slower than that of the 10^{11} Ohm amplifiers, i.e., the exponential decay time tau (τ) is much longer. As a result the apparent peak shape obtained on a 10^{13} Ohm amplifier will be asymmetrical and offset from the peak of another isotope measured simultaneously on a 10^{11} Ohm amplifier (Fig. 2). This means that cup alignment, peak centering and focusing should always be done on ion beams measured by 10^{11} Ohm amplifiers. The slower response of the 10^{13} Ohm amplifiers also implies that a much longer delay time (at least 10 sec) is needed before starting baseline or signal measurements. In addition, if signal intensities are changing rapidly a τ correction may have to be applied to account for the different

responses of signals measured simultaneously on 10^{13} and 10^{11} Ohm amplifiers (Craig et al., 2017; Kimura et al., 2016). Because of the limits on current intensity and the long decay time, amplifier rotation or multi-dynamic analyses involving both 10^{13} and 10^{11} Ohm amplifiers are not possible.

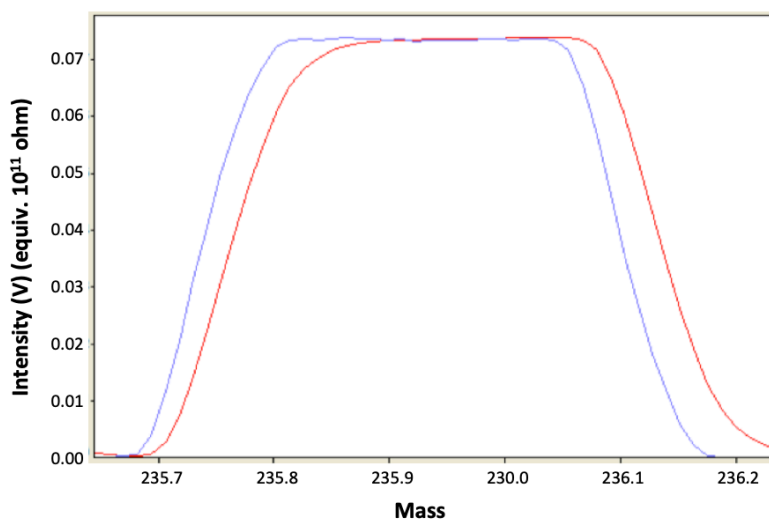


Figure 2. Apparent peak shapes of $^{188}\text{OsO}_3^-$ measured on central cup using a 10^{13} Ohm amplifier (red) and $^{190}\text{OsO}_3^-$ measured on cup H1 using a 10^{11} Ohm amplifier (blue).

Experimental set-up

The tests described here were performed by negative thermal ionization mass spectrometry (N-TIMS; (Creaser et al., 1991; Volkening et al., 1991)) at the CRPG laboratory using a Thermo Triton instrument equipped with three 10^{13} Ohm and seven 10^{11} Ohm amplifiers. Thirty analyses of 5 ng of the DROsS international Os standard were performed during three analytical sessions. Standards were loaded in HBr on Pt filaments outgassed in air for ~ 20 minutes and 0.2-0.5 μl of a saturated BaOH-NaOH solution were added to enhance formation of negative ions. Double Pt filaments were used for sessions 1 and 2; single filaments were used for session 3. Filaments were heated quite slowly (at 2 to 5 mA/min) until a measurable signal was obtained (usually at about 750 mA for double filaments, with both filaments heated at the same rate, and at about 800 mA for single filaments). Gain calibrations, lasting nearly 3 hours, were done during heating. These consisted of background readings followed by measurement of a 1.2 pA calibration current by each of the 10^{13} Ohm and 10^{11} Ohm amplifiers. In some cases long baseline measurements (2-3 hours) were also performed during sample heating. Ion beam intensities ($^{186}\text{OsO}_3^-$), averaged over the course of each run, ranged from ~ 5 fA (0.0005 V) to ~ 70 fA (0.007 V). Masses 234 ($^{186}\text{OsO}_3^-$), 236 ($^{188}\text{OsO}_3^-$), and 242 ($^{192}\text{Os}^{16}\text{O}_3^{18}\text{O}^-$) were analyzed using 10^{13} Ohm amplifiers, while masses 235 ($^{187}\text{OsO}_3^-$), 238 ($^{190}\text{OsO}_3^-$) and 240 ($^{192}\text{OsO}_3^-$) were analyzed with 10^{11} Ohm amplifiers. Though the $^{192}\text{OsO}_3^-$ signal is used in the fractionation correction and so affects the precision and accuracy of the calculated $^{186}\text{Os}/^{188}\text{Os}$ value, we chose not to measure this peak with a 10^{13} Ohm amplifier because saturation

would occur when ion beams of $^{186}\text{OsO}_3^-$ approached ~ 60 fA (0.006V), implying a $^{192}\text{OsO}_3^-$ signal of ~ 1500 fA (0.15 V). Ideally, mass 240 could be measured using a 10^{12} Ohm amplifier, but no amplifiers of this resistance were available on our instrument. We used the third 10^{13} Ohm amplifier to measure mass 242, and thus to monitor possible changes in the oxygen isotope composition. Three different cup configurations were used during the course of the analyses (Table 1).

Os peak	$^{186}\text{OsO}_3$	$^{187}\text{OsO}_3$	$^{188}\text{OsO}_3$	$^{190}\text{OsO}_3$	$^{192}\text{OsO}_3$	$^{192}\text{Os}^{16}\text{O}_2^{18}\text{O}$
Mass	234	235	236	238	240	242
Amplifier type (Ohm)	10^{13}	10^{11}	10^{13}	10^{11}	10^{11}	10^{13}
<i>Configuration A</i>						
Cup	L2	L1	C	H1	H2	H3
Amplifier #	8	1	9	3	4	10
<i>Configuration B</i>						
Cup	L3	L2	L1	C	H1	H2
Amplifier #	8	1	10	3	4	9
<i>Configuration C</i>						
Cup	L3	L2	L1	C	H1	H2
Amplifier #	8	1	9	3	4	10

Table 1. Cup and amplifier configurations used during study. Amplifiers 1 - 4 have 10^{11} Ohm resistors; amplifiers 8 - 10 have 10^{13} Ohm resistors.

Total analysis times varied between about 3 and 20 hours. Data were acquired in one or several runs, each consisting of ten blocks (in most cases). Each block was composed of ten data collection cycles, each with an integration time of 67 seconds, preceded in most cases by 10 minutes of baseline measurement. The need to measure baselines and data for approximately equal time periods in order to minimize uncertainties was stressed by Chatterjee and Lassiter (2015) for ^{186}Os analyses with 10^{11} Ohm amplifiers. Nevertheless, much of the sample is wasted during pre-block baseline measurements, so we also tested the use of shorter baselines (5 minutes prior to ~ 20 minutes of data collection) and long baseline (2-3 hours) measurements during heating and after data acquisition, as suggested by Koornneef et al. (2014) for Nd and Sr isotope measurements with 10^{13} Ohm resistors.

Wait times of 50 seconds were applied before both the baseline measurements and the first cycles of each block, to account for the long decay time of the 10^{13} Ohm amplifiers. Assuming a tau value of ~ 0.65 s, (Craig et al., 2017), a 50 second wait time is considerably longer than that (~ 9 s) which

would be theoretically needed for the signal to decrease to below 1 ppm of its original value when the ion beam is suddenly cut off. However, as can be seen in Fig. 3, which compares the response of a 10^{11} Ohm and a 10^{13} Ohm amplifier after closing the analyzer valve, the signal actually falls slightly below the baseline value before rising again. This effect was observed on all three 10^{13} Ohm amplifiers. As a result, the signal measured 10 to 20 seconds after valve closure would be systematically false by more than 100 ppm. A 50 second wait time was used to be sure to avoid this effect, though a somewhat shorter wait time (30 to 35 sec) would likely have been sufficient.

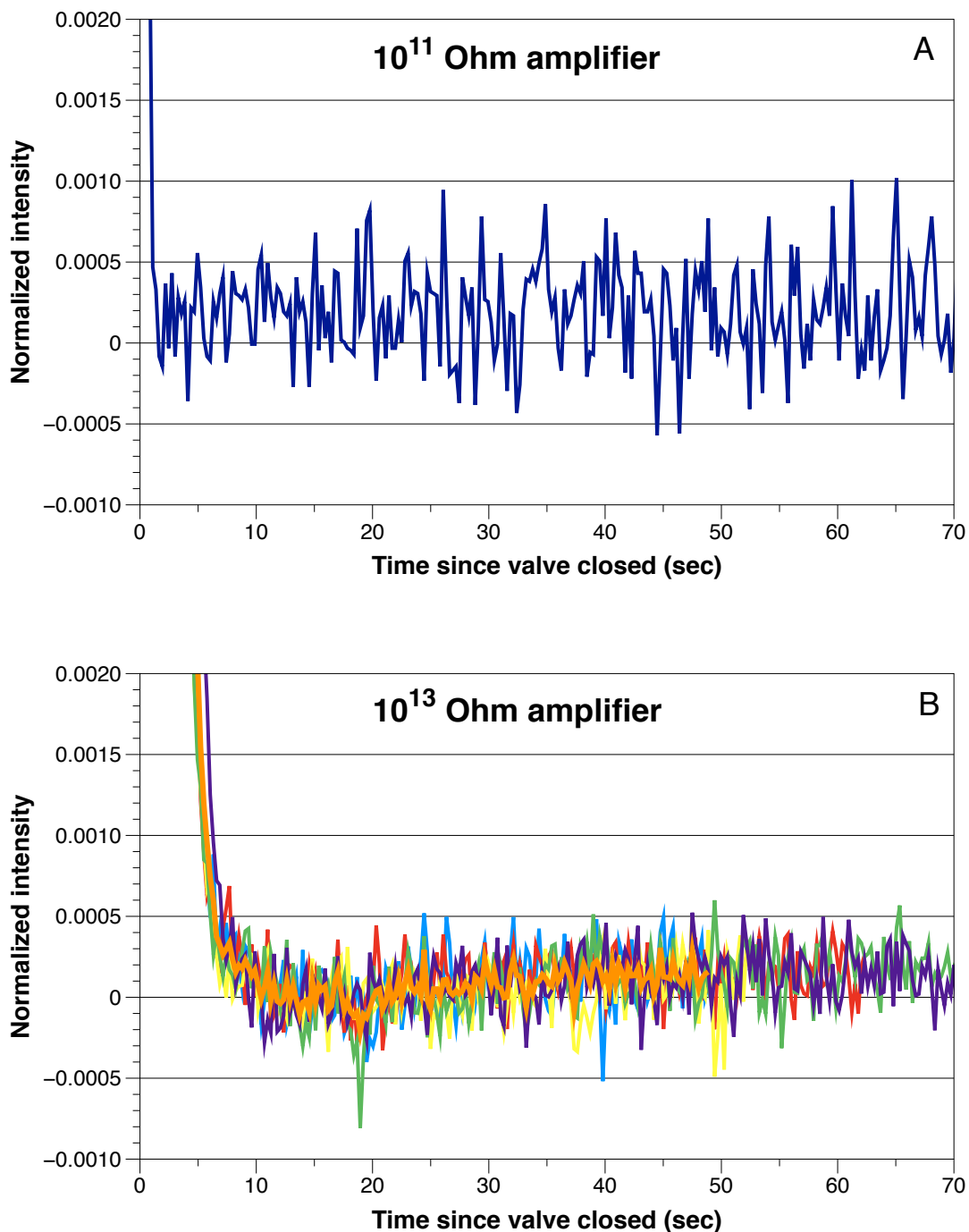


Figure 3. Comparison of response times of 10^{11} (A) and 10^{13} (B) Ohm amplifiers after closing analyzer valve. The different color traces represent repeated experiments, with the orange line representing the average. The signal intensity is normalized to the value before closing the valve.

Short interference runs were performed before and after each data collection run. These interference runs consisted of three cycles of peak jumping on the secondary electron multiplier, and included masses 228 ($^{196}\text{PtO}_2$), 230 ($^{198}\text{PtO}_2$), 231 ($^{183}\text{WO}_3$), 232 ($^{184}\text{OsO}_3$) and 233 ($^{185}\text{ReO}_3$). The $^{183}\text{WO}_3$ and $^{185}\text{ReO}_3$ measurements allow for correction of direct isobaric interferences of W and Re on ^{186}Os and ^{187}Os , respectively. However, $^{183}\text{WO}_3$ is itself subject to significant isobaric interferences from heavy oxides of PtO₂, which can be corrected through measurement of the $^{196}\text{PtO}_2$ and $^{198}\text{PtO}_2$ peaks (Luguet et al., 2008).

Data treatment

Data were exported using the "time in seconds" option of the Triton data acquisition program (Evaluate module) and opened in an Excel spreadsheet for data reduction. In some cases, discussed below, raw data without baseline and/or gain corrections were exported, and these corrections were made off-line using averaged baseline or gain values prior to further data processing. Data processing was performed in successive steps, as outlined below. In the following, "analysis" refers to the ensemble of data collected from a given filament, while "run" refers to a segment of data acquisition, normally preceded and succeeded by interference measurements.

1) **Baseline correction** (if necessary). In most cases, baselines were corrected on-line using the baseline values measured before each block. However, in a few cases (indicated as "offset"), long baselines (~ 2 hours) were measured during heating and at the end of the analysis, with much shorter baselines (5 minutes) measured prior to each 3 or 4 block run segment to monitor any possible drift. A weighted average of the baseline readings was then applied to the imported uncorrected data.

2) **Gain correction** (when gain not included in exported data). To evaluate the possible effect of spurious gain calibration values, data for each run were exported in two forms, one using the gain values obtained during filament heating prior to the analysis, and the other without gain correction. In the latter case, gain correction was performed off-line, as discussed below, using the average gain values obtained during the 5 preceding and succeeding gain calibrations.

3) **Decay time correction.** This step is used to correct for the differing response times of the 10^{13} and 10^{11} Ohm amplifiers. For the 10^{13} Ohm amplifiers used to measure the $^{186}\text{OsO}_3^-$ and $^{188}\text{OsO}_3^-$

signals a decay time (τ) of 0.65 seconds, in agreement with the τ values obtained by Craig et al. (2017), was determined by fitting an exponential curve to the signal measured after closing the analyzer valve. While small differences in the exact value of τ for different 10^{13} Ohm amplifiers can have a substantial effect on isotopic ratios obtained for rapidly varying signals, such as those measured during laser ablation experiments (Kimura et al., 2016), these are not a concern for the much more stable signals considered here. In contrast, coupling measurement of $^{188}\text{OsO}_3^-$ with a 10^{13} Ohm amplifier with the use of a 10^{11} Ohm amplifier for the $^{192}\text{OsO}_3^-$ peak can significantly bias the measured $^{192}\text{Os}/^{188}\text{Os}$ ratio and thus the mass fractionation correction if the different response times are not taken into account.

4) Isobaric interference correction. Potential isobaric interferences were estimated by interpolation based on ion counting measurements of masses 228 ($^{196}\text{PtO}_2$), 230 ($^{198}\text{PtO}_2$), 231 ($^{183}\text{WO}_3$), 232 ($^{184}\text{OsO}_3$ and $^{184}\text{WO}_3$) and 233 ($^{185}\text{ReO}_3$) performed before and after each data collection run. As a check on the ion counting results, mass 232 was also measured on the central Faraday cup, but as this cup was usually linked to a 10^{11} Ohm amplifier the Faraday data obtained for this very small peak were highly imprecise. After correction for heavy oxides, the $^{183}\text{WO}_3$ and $^{185}\text{ReO}_3$ signals and the natural isotopic compositions of W and Re were used to estimate count rates of $^{186}\text{WO}_3$ and $^{187}\text{ReO}_3$. A conversion factor of 6250 cps/fA (62500 cps/mV) was assumed to calculate the corrections to apply to masses 234 and 235 to obtain, respectively, intensities of $^{186}\text{OsO}_3$ and $^{187}\text{OsO}_3$. As most analyses were composed of several runs, interferences were usually measured several times during data acquisition.

5) Heavy oxygen correction. The interference-corrected data were then corrected for heavy oxides of OsO_3 masses by two alternative methods to allow the importance of this effect to be evaluated for each analysis. In one, the oxygen isotope composition ($^{18}\text{O}/^{16}\text{O} = 0.0020349$; $^{17}\text{O}/^{16}\text{O} = 0.0003835$) measured in a Triton mass spectrometer by Lugué et al. (2008) was assumed. In the other, the mass 242/240 ratio measured during each cycle was used to determine the $^{18}\text{O}/^{16}\text{O}$ ratio. In order to do this, it is first necessary to remove oxide interferences from the lighter Os isotopes that are isobaric with masses 240 and 242 (for example, $^{190}\text{Os}^{16}\text{O}_2^{18}\text{O}$ on mass 240). This correction requires using an assumed oxygen composition. While we used the Lugué et al. (2008) values for this second order correction, use of the Nier (1950) composition would have a negligible effect on the final result. Based on the calculated $^{18}\text{O}/^{16}\text{O}$ ratio, mass dependent fractionation was assumed to calculate the corresponding $^{17}\text{O}/^{16}\text{O}$ ratio, and the resulting values were used to correct the OsO_3 data.

6) **Mass fractionation correction.** The heavy-oxygen corrected Os isotope ratios ($^{186}\text{Os}/^{188}\text{Os}$, $^{187}\text{Os}/^{188}\text{Os}$, $^{190}\text{Os}/^{188}\text{Os}$) obtained by both methods were then corrected for mass fractionation in the instrument. An exponential law and a "true" $^{192}\text{Os}/^{188}\text{Os}$ value of 3.083 were assumed.

7) **Data combination.** If the analysis was composed of several runs these were combined to obtain the final isotope ratios and corresponding uncertainties. For analyses 28-30 a sequence of 9 short runs was programmed, with interference runs interspersed between them.

Run	Cup Set-up	Notes	Filament type	^{186}Os (mV $10^{11}\ \Omega$ amp)	Total counts ^{186}Os (10^9)	Useful yield %	$^{186}\text{Os}/^{188}\text{Os}$	$^{190}\text{Os}/^{188}\text{Os}$	$^{187}\text{Os}/^{188}\text{Os}$	$^{192}\text{Os}/^{188}\text{Os}$ measured	$^{18}\text{O}/^{16}\text{O}$
<i>Session 1</i>											
1	A	1	Double	1.39	2.05	0.8	0.1199359 0.0000089	1.983820 0.000014	0.160988 0.000014	3.077093 0.000014	0.0020155 0.0000139
2	A	1	Double	1.80	2.28	0.9	0.1199352 0.0000090	1.983720 0.000054	0.160961 0.000045	3.079254 0.000482	0.0020225 0.0000025
3	A	1	Double	3.96	4.15	1.6	0.1199273 0.0000054	1.983793 0.000035	0.160948 0.000030	3.088402 0.000703	0.0020157 0.0000006
4	A	1	Double	1.11	1.06	0.4	0.1199376 0.0000121	1.983752 0.000084	0.160880 0.000063	3.089792 0.000698	0.0020161 0.0000011
5	A	1	Double	4.14	2.98	1.2	0.1199287 0.0000060	1.983877 0.000035	0.160920 0.000026	3.082185 0.000493	0.0020109 0.0000005
<i>Session 2</i>											
6	B	1	Double	2.80	2.97	1.2	0.1199358 0.0000064	1.983879 0.000037	0.160931 0.000028	3.086256 0.000265	0.0020232 0.0000005
7	B	1	Double	4.03	1.57	0.6	0.1199425 0.0000063	1.983843 0.000036	0.160930 0.000037	3.084415 0.000386	0.0020240 0.0000006
8	B	1	Double	4.38	1.78	0.7	0.1199286 0.0000070	1.983871 0.000050	0.160954 0.000030	3.086742 0.000398	0.0020156 0.0000005
9	B	1	Double	5.92	7.06	2.8	0.1199330 0.0000036	1.983841 0.000019	0.160958 0.000013	3.085727 0.000551	0.0020195 0.0000003
10	B	1	Double	6.79	2.76	1.1	0.1199447 0.0000051	1.983815 0.000030	0.160993 0.000021	3.087846 0.000344	0.0020208 0.0000005
11	B	1	Double	5.86	2.33	0.9	0.1199321 0.0000052	1.983811 0.000031	0.160924 0.000022	3.087537 0.000289	0.0020206 0.0000006
12	B	1	Double	3.44	1.35	0.5	0.1199313 0.0000089	1.983831 0.000047	0.160989 0.000042	3.083691 0.000481	0.0020287 0.0000008
13	B	1	Double	1.95	0.93	0.4	0.1199435 0.0000139	1.983849 0.000075	0.161637 0.000133	3.082619 0.000770	0.0020287 0.0000016
14	B	1	Double	3.52	1.40	0.6	0.1199441 0.0000088	1.983923 0.000048	0.160919 0.000042	3.085349 0.000698	0.0020188 0.0000008
15	B	1	Double	3.78	1.52	0.6	0.1199408 0.0000064	1.983965 0.000047	0.160962 0.000032	3.091081 0.000268	0.0020226 0.0000006
<i>Session 3</i>											
16	B	2	Single	3.66	4.33	1.7	0.1199717 0.0000045	1.984009 0.000027	0.160924 0.000021	3.090872 0.000585	0.0020137 0.0000004
17	B	1	Single	6.90	8.21	3.3	0.1199324 0.0000039	1.984062 0.000030	0.160961 0.000015	3.093264 0.000396	0.0020061 0.0000004
18	B	1	Single	3.10	1.23	0.5	0.1199371 0.0000106	1.984021 0.000052	0.160865 0.000044	3.092825 0.000615	0.0020189 0.0000008
19	B	2	Single	3.37	1.34	0.5	0.1199661 0.0000115	1.984123 0.000055	0.160892 0.000038	3.081798 0.000616	0.0020166 0.0000009
20	B	1	Single	4.07	1.65	0.7	0.1199337 0.0000087	1.983804 0.000039	0.160933 0.000032	3.089131 0.000364	0.0020219 0.0000006

Table 2. Continued on next page.

Run	Cup Set-up	Notes	Filament type	^{186}Os (mV $10^{11}\ \Omega$ amp)	Total counts ^{186}Os (10^9)	Useful yield %	$^{186}\text{Os}/^{188}\text{Os}$	$^{190}\text{Os}/^{188}\text{Os}$	$^{187}\text{Os}/^{188}\text{Os}$	$^{192}\text{Os}/^{188}\text{Os}$ measured	$^{18}\text{O}/^{16}\text{O}$
21	B	1	Single	2.97	2.36	0.9	0.1199335 0.0000075	1.983853 0.000044	0.160904 0.000038	3.090736 0.000668	0.0020147 0.0000007
22	B	2	Single	0.47	0.19	0.1	0.1199487 0.0000419	1.983829 0.000281	0.160922 0.000253	3.092929 0.000764	0.0020148 0.0000063
23	B	2	Single	1.34	0.54	0.2	0.1199660 0.0000195	1.983822 0.000097	0.160865 0.000086	3.088025 0.000758	0.0020201 0.0000020
24	B	3	Single	1.23	0.74	0.3	0.1199465 0.0000177	1.983938 0.000089	0.160882 0.000099	3.093110 0.000414	0.0020249 0.0000015
25	B	2	Single	1.31	1.31	0.5	0.1199948 0.0000145	1.984089 0.000085	0.160917 0.000067	3.093004 0.000468	0.0020264 0.0000016
26	B	2	Single	2.21	5.70	2.3	0.1199965 0.0000056	1.983958 0.000030	0.160945 0.000025	3.094710 0.000329	0.0020106 0.0000005
27	C	4	Single	3.19	3.57	1.4	0.1199472 0.0000065	1.984092 0.000064	0.161132 0.000017	3.089300 0.000667	0.0020136 0.0000003
28	C	1, 5	Single	5.64	5.46	2.2	0.1199400 0.0000038	1.984123 0.000022	0.160966 0.000015	3.087470 0.000651	0.0020130 0.0000004
29	C	1, 5	Single	2.29	1.94	0.8	0.1199373 0.0000077	1.983999 0.000054	0.160947 0.000038	3.085441 0.000760	0.0020110 0.0000008
30	C	1, 5	Single	5.61	7.97	3.2	0.1199393 0.0000033	1.984144 0.000020	0.161020 0.000012	3.087543 0.000365	0.0020065 0.0000005
<i>Average ("1" runs)</i>				3.88	2.95	1.1	0.1199361	1.983891	0.160977	3.086564	0.0020180
<i>2 Std. deviations</i>				3.37	4.43	1.7	0.0000102	0.000230	0.000304	0.008059	0.0000123
<i>2 S.D. (ppm)</i>							85	116	1887	2611	6105

- 1: Included in average - No obvious anomalies
2: Excluded from average - Interference correction on $^{186}\text{Os}/^{188}\text{Os} > 0.0000100$
3: Excluded from average - Signal dying rapidly so heated between each block
4: Excluded from average - Short baselines
5: Included in average - Offset backgrounds

Table 2. Results of thirty analyses of the DROsS international Os standard. Data have been corrected as detailed in text for gain variations using average values, amplifier decay times, interpolated isobaric interferences, in-run measured oxygen compositions and mass fractionation (except $^{192}\text{Os}/^{188}\text{Os}$). For analyses 1-26, baselines of 10 minutes were measured prior to each block of ~11 minutes; for analysis 27 baselines of 5 minutes were measured before each two blocks; for analyses 28-30 long baselines of ~2 hours were performed during heating and after data acquisition, with 5 minute baselines before every 3 or 4 block run. Cup configurations (A,B,C) are defined in Table 1. Ratios included in average (detailed in Table footnotes) include those analyzed with 10 minute pre-block backgrounds or with offset backgrounds that were not subject to large interference corrections.

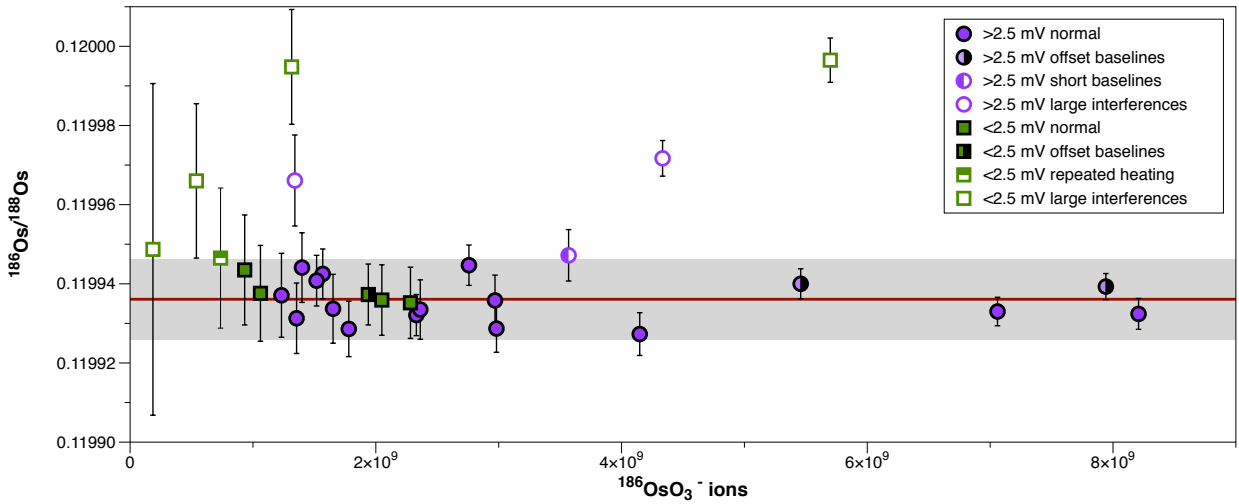
Results

Table 2 lists results for the thirty analyses performed in this study. $^{186}\text{OsO}_3^-$ beam intensities varied from 5 to 69 fA (0.0005 to 0.0069 V equiv. 10^{11} Ohm amplifier), while the number of $^{186}\text{OsO}_3^-$ ions measured varied from 0.2 to 8.2×10^9 , corresponding to useful Os yields of 0.1 to 3.3 %. These calculated yields include only those ions actually used for data acquisition; they do not include ions emitted during focussing, centering, wait times, or background and interference measurements.

They also do not include the ions arriving at the beginning and ends of measurements, when the $^{186}\text{OsO}_3^-$ beams are considered too small (usually $<10\text{fA}$; 0.001V) for acquisition of useful data.

In Fig. 4 the $^{186}\text{Os}/^{188}\text{Os}$ ratios obtained after all data corrections are shown as a function of the number of measured ^{186}Os ions. Analyses run under standard conditions for which no obvious anomalies were observed ("normal", filled symbols), together with analyses with "offset" baselines (half-black symbols), have an average $^{186}\text{Os}/^{188}\text{Os}$ ratio of 0.1199361 ± 0.0000102 (2σ ; 85 ppm), in agreement with previously published high precision analyses of the DROsS standard (Chatterjee and Lassiter, 2015; Chu et al., 2015; Liu and Pearson, 2014; Lugué et al., 2008). The half-filled violet circle represents an analysis done with short baselines, while the half-filled green square denotes a filament that was substantially heated (filament current increased by 5 to 10 mA) before each block. The open symbols represent analyses requiring unusually large interference corrections. It is clear that even after interference correction, these latter samples often have $^{186}\text{Os}/^{188}\text{Os}$ ratios exceeding the normal range.

A)



B)

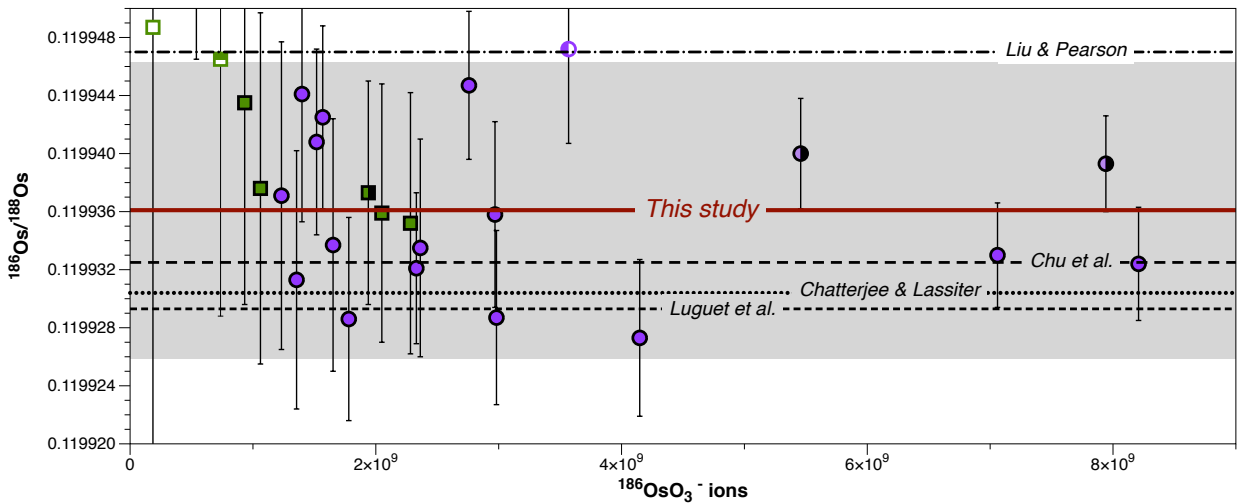


Figure 4. A) $^{186}\text{Os}/^{188}\text{Os}$ ratios as a function of number of $^{186}\text{OsO}_3^-$ ions measured, after all data corrections. Analyses with ^{186}Os signals less and greater than 2.5 mV (equiv. on 10^{11} Ohm amplifier) are distinguished. The deep red horizontal line and the gray shaded area represent the average and 2σ variation of the "normal" analyses and of analyses with offset baselines (baselines measured primarily during heating and after analysis). B) Expanded view of (A) comparing results of this study with those of previous studies that analyzed the DROsS standard (Luguet et al., 2008; Liu and Pearson, 2014; Chu et al., 2015; Chatterjee and Lassiter, 2015).

Fig. 5A shows the internal precision of each analysis (1 standard error) as a function of the number of ^{186}Os ions reaching the collectors. To facilitate comparison with the theoretical curves, the data are divided into samples with average ^{186}Os beam intensities greater and less than 25 fA (2.5 mV). These are compared to the theoretical limits of precision imposed by the combination of counting statistics and of Johnson-Nyquist noise. The counting statistic limit in ppm, defined by the equation:

$$rsd_{CS} = 10^6 \times \sqrt{\frac{1}{cts_{186}} + \frac{1}{cts_{188}}} \quad (2)$$

reflects the random variation of ion arrivals and depends uniquely on the total number of ions measured (cts_{186} and cts_{188} , for ^{186}Os and ^{188}Os respectively). Equation 3 expresses the limit on precision imposed by the Johnson-Nyquist effect:

$$rsd_{JN} = 10^6 \times \sqrt{\frac{\left(\frac{V_{JN}}{V_{186}}\right)^2 + \left(\frac{V_{JN}}{V_{188}}\right)^2}{n}} \quad (3)$$

Here, V_{JN} is the J-N noise in V calculated by Eq. 1, V_{186} and V_{188} are the signal intensities in V of the ^{186}Os and ^{188}Os beams, and n is the number of integrations. Unlike the uncertainty related to counting statistics, that due to J-N noise depends on both the total number of ions measured (through n and V_{JN} , which includes the integration time, t ; see eq. 1) and on the intensities of the ion beams. Fig. 5B shows separately the uncertainties predicted from counting statistics and from J-N noise for ion beams of three different beam intensities (10, 30 and 50 fA, corresponding to 1, 3 and 5 mV on 10^{11} Ohm amplifiers) in the range of the signal sizes of the analyzed standards.

In Fig. 5A the J-N noise is combined with the counting statistic curve to obtain the total theoretical precision limit (rsd_{tot}) for each of these three beams, using the equation:

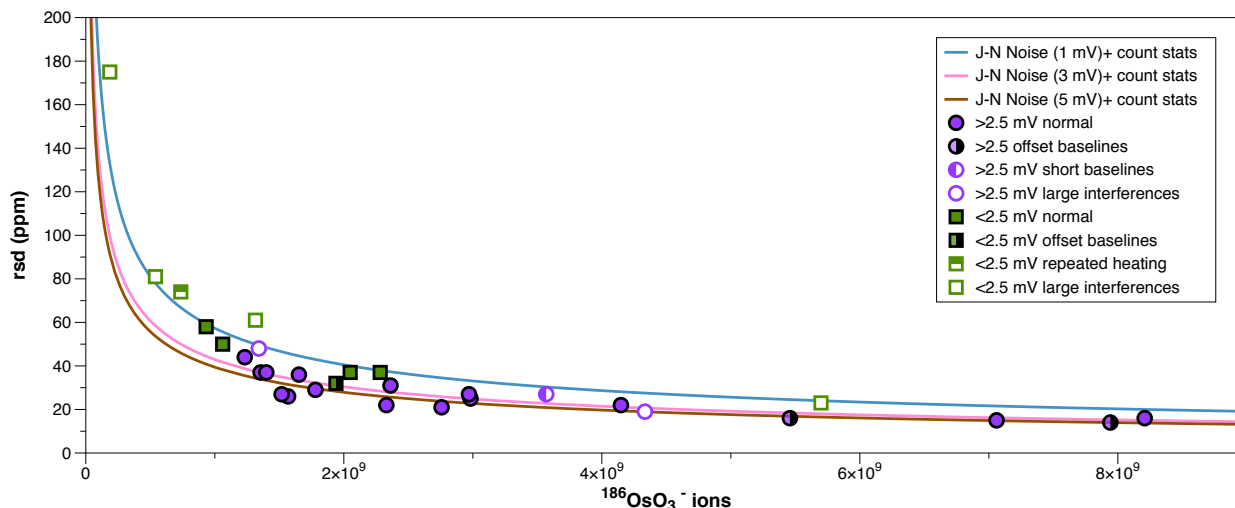
$$rsd_{tot} = \sqrt{(rsd_{CS})^2 + (rsd_{JN(S)})^2 + (rsd_{JN(B)})^2} \quad (4)$$

where rsd_{CS} , $rsd_{JN(S)}$ and $rsd_{JN(B)}$ represent, respectively, the standard deviations related to counting statistics, J-N noise on the signal and J-N noise on the baseline. As the total measurement times for baseline and signal were approximately the same, $rsd_{JN(S)}$ and $rsd_{JN(B)}$ will be about equal. Analyses without large interference corrections have standard errors approaching the theoretical limits. This suggests that sources of in-run uncertainties other than counting statistics and JN noise are quite small. In particular this suggests that in-run uncertainties related to the fractionation correction, which are not considered in eq. 4, are insignificant.

While the analytical precisions are about as good as can be theoretically expected, this may not be true of the reproducibility. As the analyses spanned a wide range of signal intensity and run length, the expected reproducibility is difficult to estimate. To obtain a rough approximation, we consider the median intensity (0.0037 V) and the median number of counts (2×10^9) of ^{186}Os in the runs without obvious anomalies (labelled "1" in Table 2). In this case, the 2σ uncertainty calculated from J-N noise and counting statistics would be about 58 ppm. If this approximation is valid, it would

suggest that the theoretical reproducibility of the $^{186}\text{Os}/^{188}\text{Os}$ ratio is significantly better than the observed 2σ variation (85 ppm) over the duration of the study, and could indicate that factors other than J-N noise and counting statistics led to minor variations between runs. One of these could potentially be degradation of the Faraday cups over the period of the study.

A)



B)

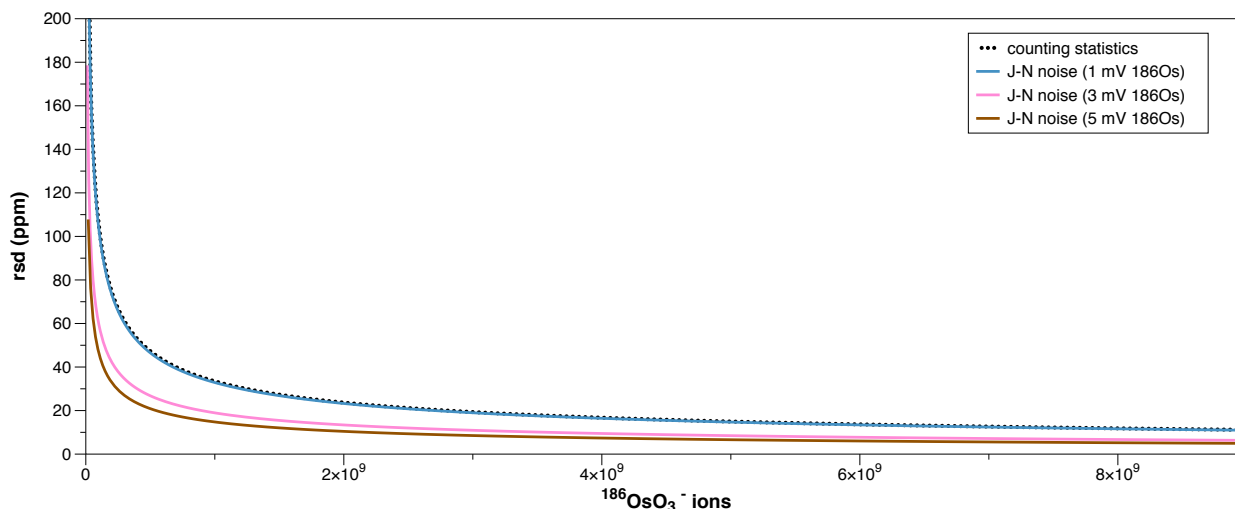


Figure 5. A) Uncertainties (1 rsd) on $^{186}\text{Os}/^{188}\text{Os}$ data as a function of number of $^{186}\text{OsO}_3^-$ ions measured. Data are compared with noise levels theoretically predicted from the combination of uncertainties from counting statistics and Johnson-Nyquist noise (including effect on both signal and baseline). As the relative J-N uncertainties depend on both the total number of ions measured and the intensity of the signal, curves are shown for three different signal intensities pertinent to our study. B) J-N uncertainties (1 rsd) predicted for ^{186}Os signal intensities from 1- 5 mV (equiv. 10^{11} Ohm amplifier) and uncertainties related to counting statistics. The curve for counting statistic uncertainties is very similar to that for J-N noise for 1 mV signals.

In addition to listing results for $^{186}\text{Os}/^{188}\text{O}$ ratios, Table 2 also presents data for $^{190}\text{Os}/^{188}\text{Os}$ and $^{187}\text{Os}/^{188}\text{Os}$, for which the isotope peak in the numerator was measured with a 10^{11} Ohm amplifier. The average $^{190}\text{Os}/^{188}\text{Os}$ ratio obtained (1.983891 ± 0.000230 , 2σ) agrees with results from previous analyses of the DROsS standard (Chatterjee and Lassiter, 2015; Liu and Pearson, 2014; Luguet et

al., 2008), though the uncertainty is larger than in those studies because of the order of magnitude difference in signal size. The average $^{187}\text{Os}/^{188}\text{Os}$ ratio (0.160977 ± 0.000304) also agrees with literature data, but the uncertainty is quite large. Comparison of the relative uncertainty of this ratio (1887 ppm) with that of the $^{186}\text{Os}/^{188}\text{Os}$ ratio (85 ppm) suggests that this uncertainty is at least two or three times larger than would be expected simply because of the use of a 10^{11} rather than a 10^{13} Ohm amplifier to measure $^{187}\text{OsO}_3$. We suspect that this points to the presence of minor unidentified molecular interferences that are not removed by the interference correction routine.

Discussion

Each of the factors that potentially affect the precision and reproducibility of the isotopic results are considered below.

Useful yields

The most direct factor controlling the precision of the results is the number of OsO_3^- ions measured. In these tests, one of our major concerns was avoiding systematic biases, so very conservative choices were made concerning run parameters. Thus it is possible that some improvement in usable yield could be made by decreasing wait times, minimizing the length (but not the frequency) of interference analyses, and limiting the frequency of focusing and centering. Performing long baseline analyses before and after the run also increases the useful yield, but as discussed below, shorter in-run baseline monitoring is still advisable to catch possible systematic drift. Analyses 28 and 30, two of the three analyses run with baselines offset in time in this manner, have among the highest useful yields and correspondingly low 2SE uncertainties. Another factor that likely improved the yield in these cases was that the 10 interference runs and 9 data collection runs comprising each of analyses 28-30 were programmed in an automatic run sequence, thus eliminating possible time lost during user intervention. Nevertheless, further tests are needed to optimize the loading parameters required to assure large stable ion beams, as this is critical to achieving high yields.

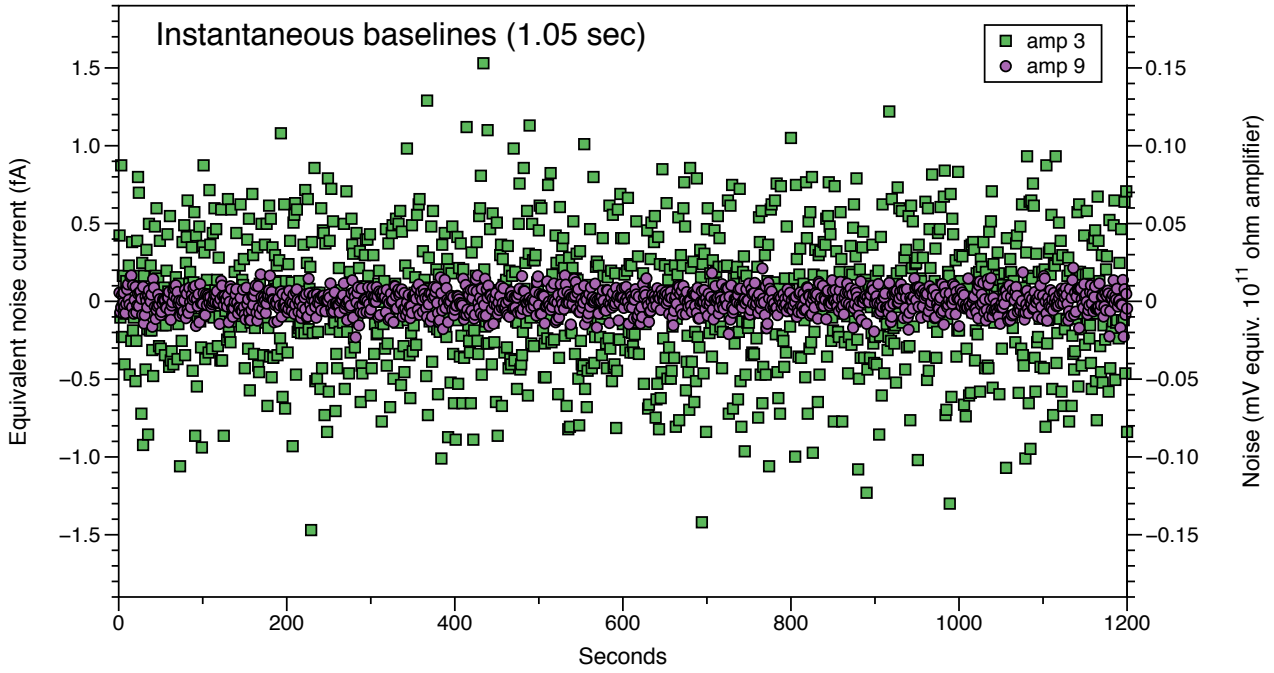
In this context, it is interesting to consider the theoretical minimum amount of osmium required to obtain $^{186}\text{Os}/^{188}\text{Os}$ data of a given precision. To obtain a precision (1 rsd) of 25 ppm, Fig. 5A indicates that $\sim 2.4 \times 10^9$ atoms of ^{186}Os would have to be measured, assuming that a signal intensity of 50 fA (0.005V) could be maintained. This corresponds to $\sim 2.5 \times 10^{-13}$ moles of total Os, or 0.048 ng. Assuming that 5% of the ^{186}Os atoms loaded on the filament are actually measured by the collector, this means that the minimum amount of Os needed to obtain 25 ppm precision would be \sim

0.96 ng. In contrast, if a precision (1 rsd) of 10 ppm is required, $\sim 1.43 \times 10^{10}$ atoms of ^{186}Os must be measured, corresponding to ~ 5.6 ng of Os loaded on the filament using the same assumptions. Conversely, if 3 ng of Os are loaded, it is not possible to obtain better than 14 ppm precision. Furthermore, an assumption of 5% useful yield is rather optimistic, and exceeds the values obtained in our experiments (Table 2). Also, as discussed above, in-run precision is often less good than reproducibility, which is of more interest. Nevertheless, for a known amount of Os deposited on the filament, this simple calculation provides some insight into the theoretical optimum result that could be hoped for.

Baselines

The analytical baselines of 10^{11} and 10^{13} Ohm amplifiers are compared in Fig. 6, and short term (1.05 s baselines measured successively over 2 hours) and long term (mostly 10 minute baselines measured sporadically over 6 weeks) variations for each of the amplifiers are listed in Table 3.

A)



B)

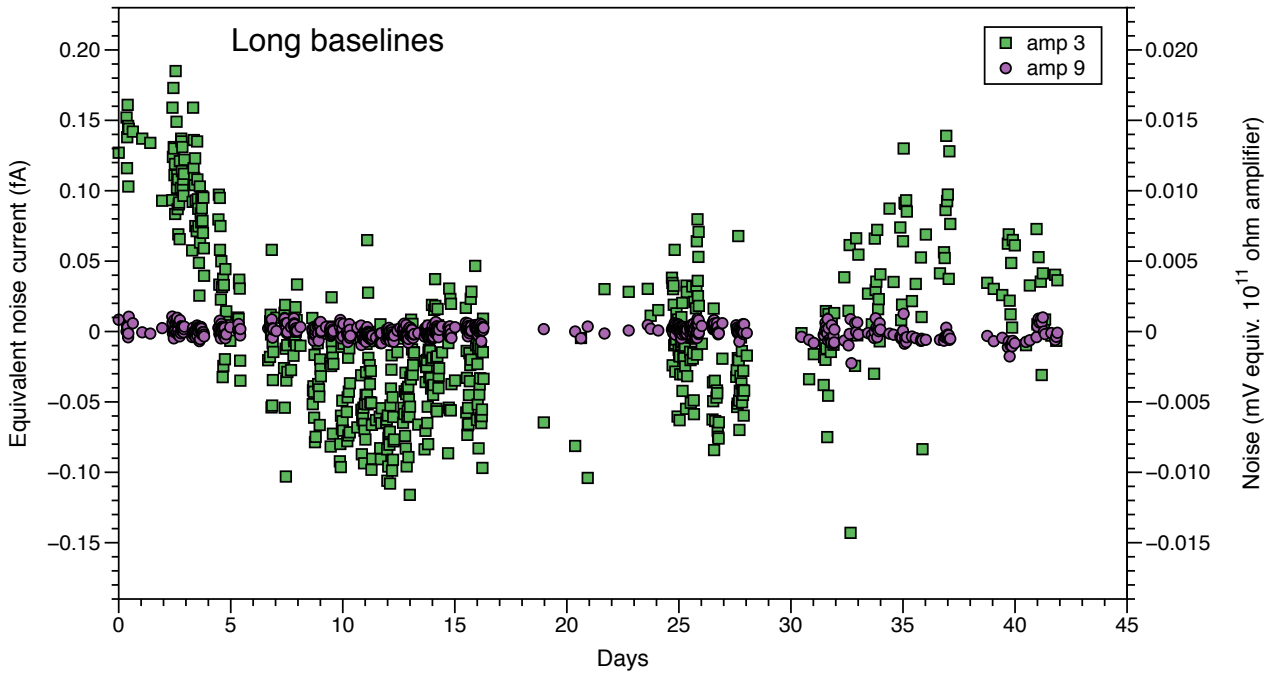


Figure 6. Comparison of baselines measured on 10^{11} Ohm (amp 3) and 10^{13} Ohm (amp 9) amplifiers over short (~ 20 minute) and long (6 week) periods. To facilitate comparison, the average baseline reading over the period considered has been subtracted. A) Results of 1200 successive 1.05 second baseline readings; B) Results of baseline measurements averaged over long time periods (mostly 10 minutes) during and prior to analyses and during gain calibrations.

Using Eq. (1), it can be calculated that the Johnson-Nyquist noise associated with 10^{11} Ohm resistors should be about 0.04 mV (0.4 fA) for successive baseline readings of 1.05 seconds, which is approximately equal to the variability (1σ) observed for the 10^{11} Ohm amplifiers (Table 3). The J-N noise associated with 10^{13} Ohm resistors should be about 0.4 mV, equivalent to 0.04 fA (0.004 mV on a 10^{11} Ohm amplifier). The observed baseline variability for the 10^{13} Ohm amplifiers is

about 0.07 fA, that is, it is improved by a factor of 5 or 6 relative to what is obtained with the 10^{11} Ohm amplifiers, which contrasts with the factor of 10 improvement that might be expected. Similar slightly sub-optimal performance has been found in previous studies of these amplifiers (Koornneef et al., 2014). This may suggest that a small amount of the noise in the 10^{13} Ohm amplifiers is derived from sources other than the feedback resistor.

Amplifier #	1	3	4	8	9	10
Resistance (Ohm)	10^{11}	10^{11}	10^{11}	10^{13}	10^{13}	10^{13}
<i>7200 successive 1.05 s baseline readings</i>						
Std dev. (mV)	0.0384	0.0406	0.0391	0.6918	0.6859	0.7071
Std dev. (fA)	0.3845	0.4058	0.3914	0.0692	0.0686	0.0707
<i>Long baselines (mostly 10 min) during 6 week period</i>						
Std dev. (mV)	0.0082	0.0060	0.0056	0.0366	0.0422	0.1333
Std dev. (fA)	0.0818	0.0595	0.0556	0.0037	0.0042	0.0133
<i>Gains during 6 week period</i>						
Average	1.005229	0.979885	0.996887	0.0101606	0.0099345	0.0103439
Std dev.	0.000201	0.000212	0.000208	0.0000021	0.0000021	0.0000022
Std dev. normalized	0.000048	0.000041	0.000056		0.000012	0.000013

Table 3. Baseline and gain variations of the three 10^{11} and three 10^{13} amplifiers used in this study. For the baselines, mV refers to the absolute variation measured on the amplifier (ie, not normalized to the resistance). For the gains, "Std dev. normalized" means the standard deviation of the individual gains on amp x normalized first to the corresponding gains on amp 8 (gain(x)/gain(8)) and then to the average value of gain(x)/gain(8).

Fig. 6B compares longer term baseline variations in typical 10^{11} and 10^{13} Ohm amplifiers. Most of the points shown were 10 minute baselines measured before each block of data collection, though some points represent baselines measured during gain calibrations or long baselines measured between sample analyses. It is clear that the 10^{11} Ohm amplifiers display substantial long term drift not observed with the 10^{13} Ohm amplifiers. Nevertheless, when looked at in detail (Table 3), it appears that one of the 10^{13} Ohm amplifiers (amp 10) displays about three times as much variation as the other two 10^{13} Ohm amplifiers (amps 8 and 9). This greater variation is not random, but instead reflects medium term drift in amp 10 occurring during many of the runs. As seen in Fig. 7, which shows an expanded view of 10 days of variation of the baselines of each of the 10^{13} Ohm amplifiers, the baseline value of amp 10 seems to be reset to a high value during the gain calibration preceding each analysis, and then to gradually decrease during the run. This drift is not always observed, but when it is, it appears to occur at a rate of about -1×10^{-5} mV (equiv. 10^{11} Ohm amplifier) per minute. For the typical case of ~ 12 minutes between the start of the baseline reading and the start of data acquisition in each block, this translates to an overcorrection of about 1.2×10^{-4}

mV (equiv. 10^{11} Ohm amplifier). Amplifier 10 was never assigned to the $^{186}\text{OsO}_3$ peak, and in most cases (Table 2) was used to measure the $^{188}\text{OsO}_3$ peak, which almost always had an intensity > 10 mV. This means that the effect of this drift was usually less than ~ 10 ppm, and was always well within the limits of uncertainty. Nevertheless, these observations underscore the importance of carefully tracking possible baseline drift, even when the short term noise of the amplifier appears normal (Table 3).

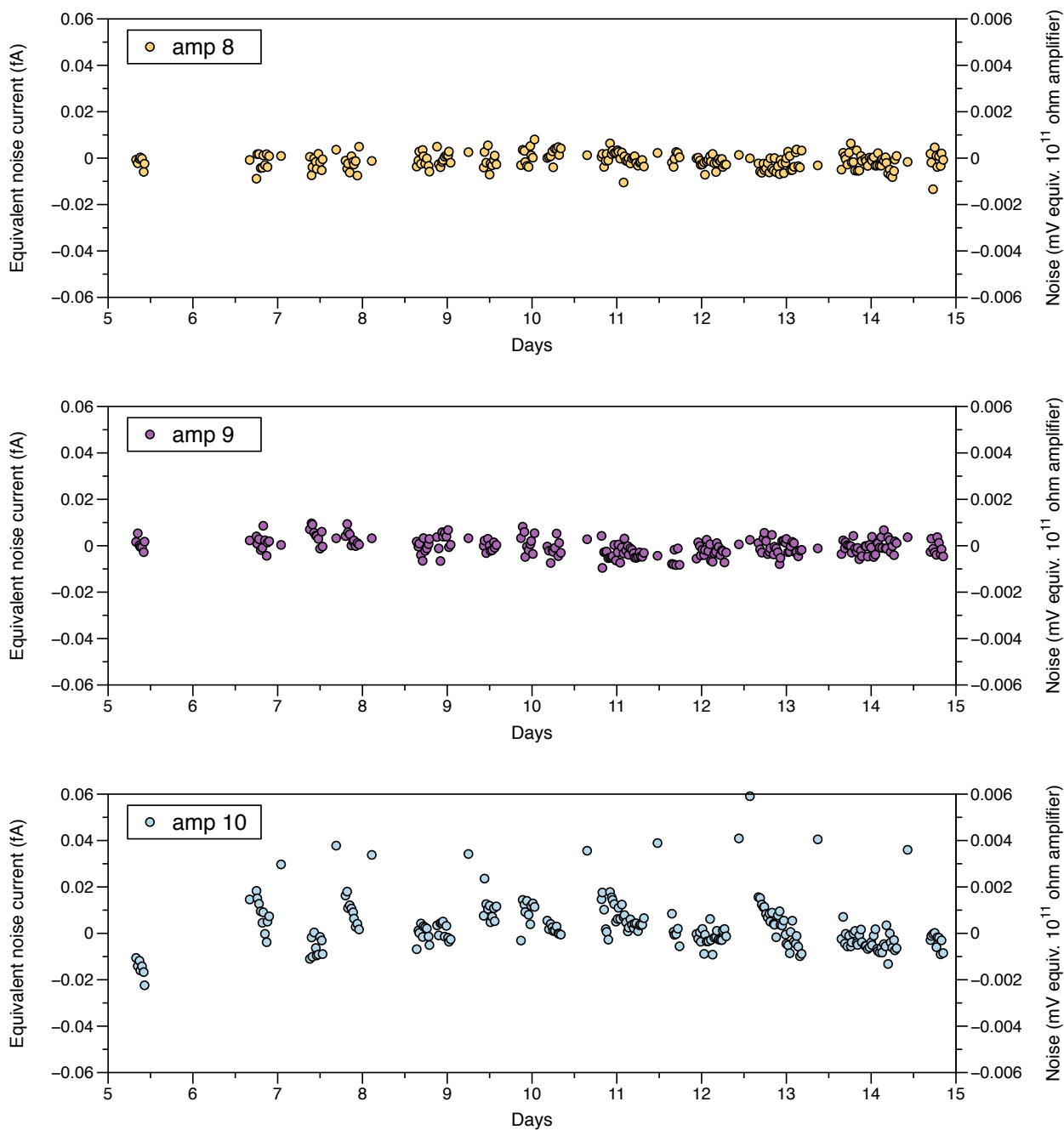


Figure 7. Expanded view of baselines measured on the 10^{13} Ohm amplifiers during a 10 day period. For amplifier 10, the isolated points plotting above 0.02 fA correspond to baselines measured during gain calibrations while the negatively sloping segments correspond to baselines preceding blocks during analyses.

Chatterjee and Lassiter (2015) emphasized that in order to obtain high precision data it is just as important to reduce the uncertainty associated with Johnson-Nyquist noise on the baseline as it is to reduce the J-N uncertainty of the signal itself. For this reason, for most of our analyses baselines and signal were measured for approximately equal amounts of time, with a baseline reading of about 10 minutes preceding each ~10 minutes of signal measurement. As can be seen in Fig. 5A, this procedure produced $^{186}\text{Os}/^{188}\text{Os}$ ratios with precisions close to those theoretically predicted from the combination of uncertainties related to counting statistics and to J-N noise on the signal and on the baseline. Moreover, the average $^{186}\text{Os}/^{188}\text{Os}$ ratio of the DROsS analyses performed in this manner (ie, excluding analyses 27-30) was 0.1199357 ± 0.0000108 (2σ), in agreement with values found in the literature. Nevertheless, long baseline analyses prior to each block are wasteful of sample material, so we explored possible alternative approaches (runs 27-30). In these tests, the slightly questionable amplifier 10 was used only to measure the heavy oxygen composition and thus does not bias the results. In run 27, baselines were measured for only 5 minutes prior to each 20 minute period of signal analysis. As can be seen in Fig. 4 ("short baselines"), the $^{186}\text{Os}/^{188}\text{Os}$ ratio of this analysis plots slightly outside (though within error of) the field defined by the samples with long pre-block backgrounds. In three runs (28-30) long baselines (2-3 hours) were measured during sample heating and after analysis, after the suggestion of Koornneef et al. (2014), who successfully used this approach for the analysis of small loads of Sr and Nd with 10^{13} Ohm amplifiers. In addition, short baselines (5 minutes) were measured prior to each 30 minute segment of data acquisition to monitor any possible drift during the analysis. A weighted average of all of the long and short baseline measurements was then subtracted off-line from the uncorrected data. The $^{186}\text{Os}/^{188}\text{Os}$ ratios of these three analyses agreed with the values obtained by our normal procedure of ten minute baselines preceding each block (Fig. 4), and the precisions were equal to those expected from theoretical considerations. Thus long pre- and post-analysis baseline measurements provide an effective means of avoiding sample waste. Nevertheless, given the systematic in-run drifts in baseline observed on amplifier 10, and the strong possibility that similar drifts may occur on 10^{11} Ohm amplifiers, it is advisable to couple pre- and post-analysis baselines with shorter, periodic baselines during data acquisition to monitor any such effects. It is also important to carefully control medium to long term baseline variations.

Gains

Gain calibration is complicated by the need to use a calibration current that can be measured accurately by both 10^{11} and 10^{13} Ohm amplifiers. For negative ions, a calibration current of 1.2 pA is used. This corresponds to 12 V, which is nearly full scale, on a 10^{13} Ohm amplifier. If the gain pulse and the associated baseline are both measured for 10 minutes, the J-N noise on the resistor

would lead to an uncertainty of only about 2 ppm. In contrast, the same calibration current would be measured as 0.12 V on a 10^{11} Ohm amplifier, and the J-N noise would correspond to an uncertainty of about 20 ppm, which is not completely negligible. This rough calculation is not expected to match the variability obtained in actual gain calibrations performed sporadically over a several week period, but nevertheless shows why this effect should be considered in measurements employing a mixed array of 10^{11} and 10^{13} Ohm amplifiers. This problem is less severe for positive ions, as the calibration current is 3.3 pA (0.33 V equiv. 10^{11} Ohm amplifier).

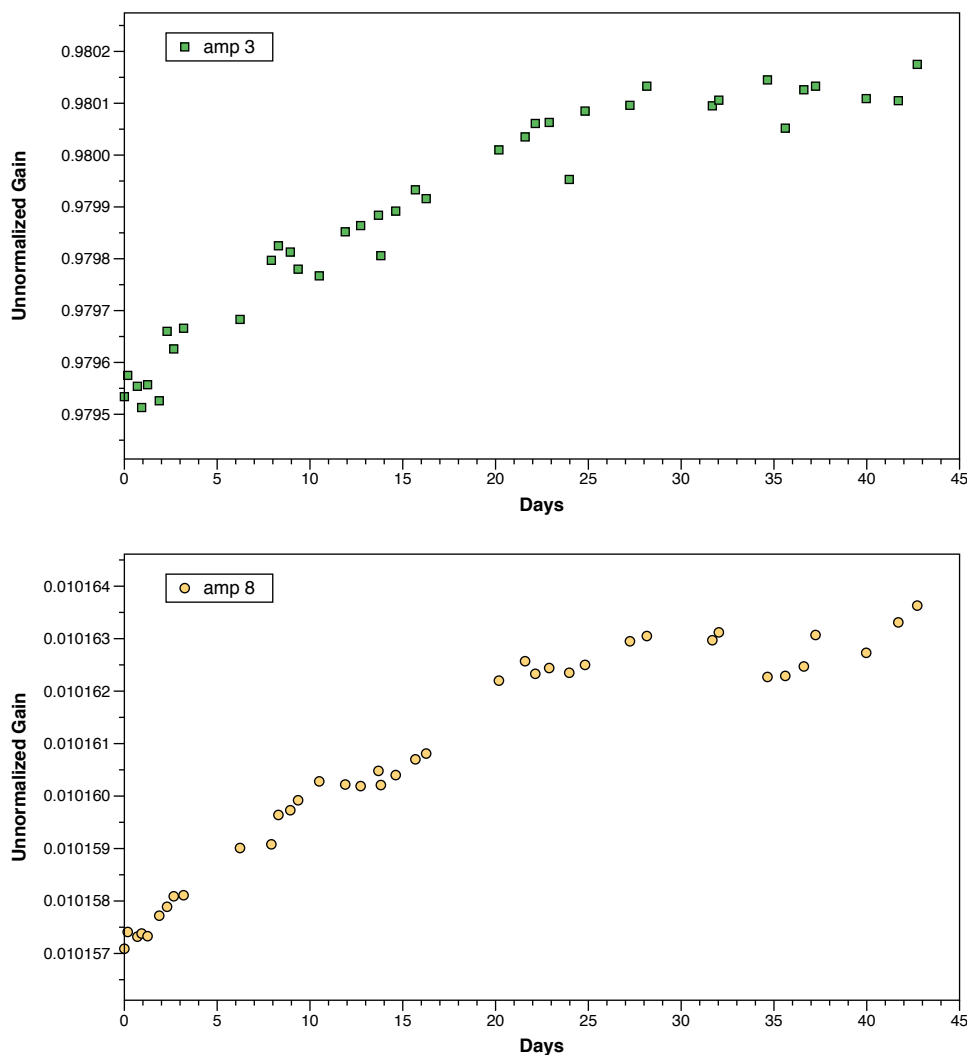


Figure 8. Variation of measured gain of typical 10^{11} Ohm (amp 3) and 10^{13} Ohm (amp 8) amplifiers over a six week period.

The average gain values obtained over a six week period are listed in Table 3, and plots of the gain variations of representative 10^{11} Ohm (amp 3) and 10^{13} Ohm (amp 8) amplifiers during this time are shown in Fig. 8. As the relative variations are of much more interest than the absolute variations, in Fig. 9 all of the gains have been normalized to that of amplifier 8, the 10^{13} Ohm amplifier used to measure $^{186}\text{OsO}_3$ in all cases. This plot shows that individual gain calibration values (normalized to amp 8) of the 10^{11} Ohm amplifiers can vary by as much as 100 ppm (relative standard deviations of

48, 41 and 56 ppm for amps 1, 3 and 4 respectively, Table 3). In contrast, the relative gain variations of the 10^{13} Ohm amplifiers are much smaller (12 and 13 ppm). No statistically significant long term drift in the relative gain is observed for either type of amplifier, though all amplifiers show substantial long term absolute gain drift (~ 750 ppm) over the six week period (Fig. 8).

In all of the tests, both $^{186}\text{OsO}_3$ and $^{188}\text{OsO}_3$ were measured using 10^{13} amplifiers so the direct effect of gain variations on the $^{186}\text{Os}/^{188}\text{Os}$ ratio should be small. However, the $^{192}\text{OsO}_3$ peak which is used for the mass fractionation correction is measured on a 10^{11} Ohm amplifier. An error of 100 ppm on the gain calibration of this amplifier would lead to an error of about 50 ppm on the mass bias corrected $^{186}\text{Os}/^{188}\text{Os}$ ratio. To judge the effect of random gain variability on the final results, data reduction was performed for each sample using both the gain measured during filament heating before analysis, and the average of the five preceding and five subsequent gain measurements. As shown in Table 4, the use of averaged rather than individual gains improves the overall reproducibility of the $^{186}\text{Os}/^{188}\text{Os}$ ratio by about 12 ppm. Thus using averaged gain values can lead to a small, but non-negligible improvement in reproducibility, and can eliminate outlier values caused by spurious individual calibrations.

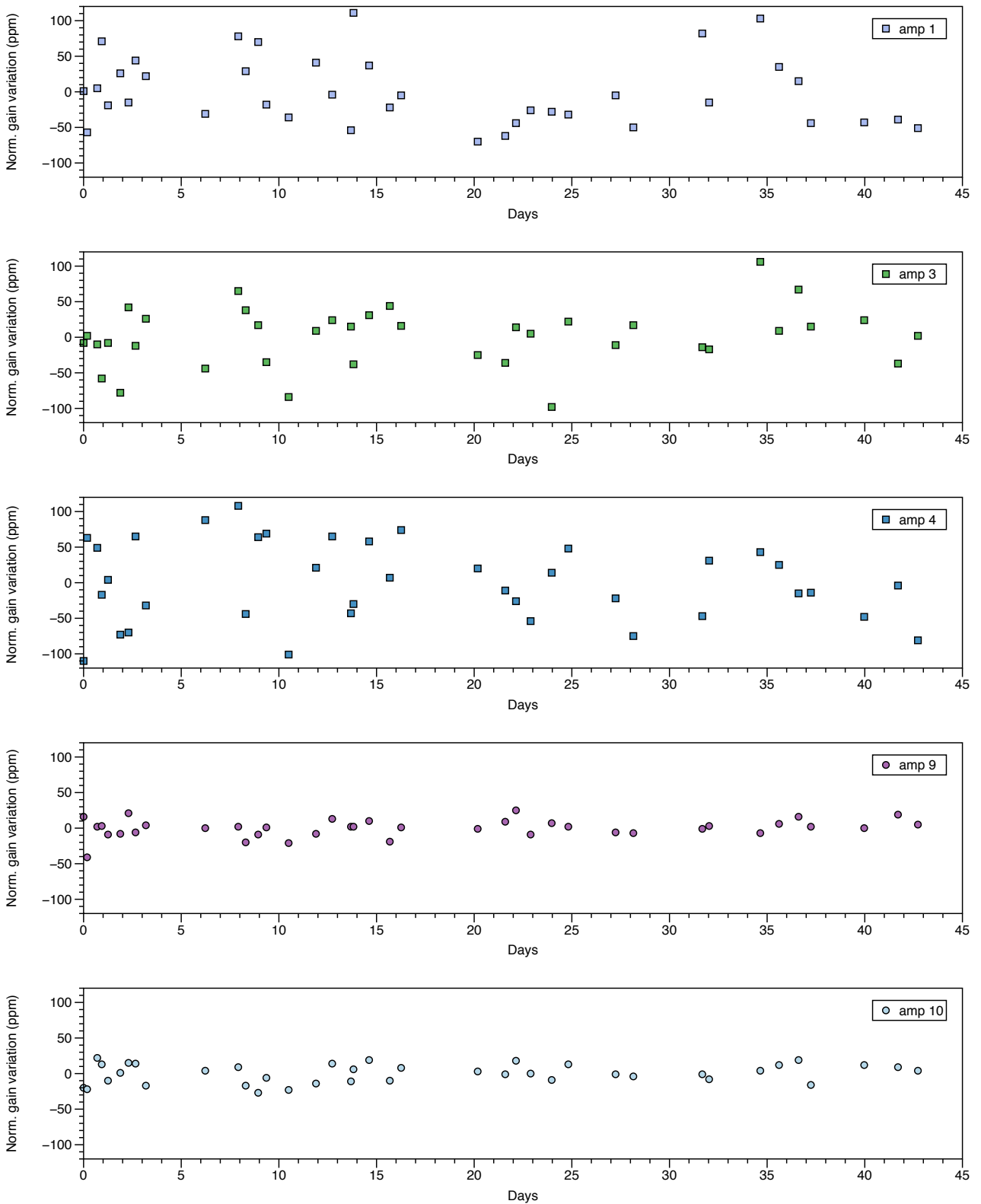


Figure 9. Variations (in ppm) of gains of 10^{11} Ohm amplifiers (amps 1, 3 and 4) and 10^{13} Ohm amplifiers (amps 9 and 10) normalized to gain of amp 8 (10^{13} Ohm). To facilitate comparison the ratio $\text{gain}(x)/\text{gain}(8)$ is normalized to the average value over the six week period.

	Change in $^{186}\text{Os}/^{188}\text{Os}$ (Range)	Change in $^{186}\text{Os}/^{188}\text{Os}$ (Average)	Range of change ppm	Average change ppm	Effect on overall variability (ppm change in 2σ of all analyses)
Gain averaging	-0.0000065 to 0.0000065	-0.0000001	-54 to 54	-1	-12
Decay time correction	-0.0000010 to 0.0000087	0.0000023	-8 to 72	19	+2
Individual vs. fixed O2 correction	0.0000002 to 0.0000020	0.0000008	2 to 17	7	+1
Interferences (all runs)	0.0000003 to 0.0000639	0.0000092	3 to 533	77	
Interferences (good only - see caption)	0.0000003 to 0.0000058	0.0000029	3 to 48	24	
Interferences (single filaments)	0.0000024 to 0.0000639	0.0000151	20 to 533	126	
Interferences (double filaments)	0.0000003 to 0.0000045	0.0000015	3 to 38	13	

Table 4. Effects of various factors on final calculated $^{186}\text{Os}/^{188}\text{Os}$ ratios. The range and the average value of the change in $^{186}\text{Os}/^{188}\text{Os}$ caused by the considered factor are shown, in both absolute and relative values (ppm). The effect on the overall variability of the ensemble of measurements is also shown. The analyses indicated as "good" were defined as those for which the calculated interference correction to $^{186}\text{Os}/^{188}\text{Os}$ was less than 0.000100 (24 analyses).

Decay time effects

The long decay time of the 10^{13} Ohm amplifiers will lead to biases in measured values for ion beams of varying intensity, with the direction and extent of the bias depending respectively on whether the signal is increasing or decreasing and on the slope of this change. As the decay time of 10^{11} Ohm amplifiers is insignificant isotopic ratios obtained with a combination of 10^{11} and 10^{13} Ohm amplifiers can be systematically inaccurate. This observation is applicable to the $^{192}\text{Os}/^{188}\text{Os}$ ratios used for mass bias correction in our study. Fortunately, as the extent of bias depends uniquely on the slope of the signal change and the value of the decay time, τ , this effect can be corrected for using equation 5, which can be simply derived from the exponential decay equation (Craig et al., 2017; Kimura et al., 2016).

$$I_t = I_m + \frac{I_{m+1} - I_{m-1}}{t_{m+1} - t_{m-1}} \times \tau \quad (5)$$

Here I_m and I_t refer respectively to the measured and true signal intensities of a given measurement cycle. As evident from eq. 5, the slope at the time (t) of each measurement is obtained from the preceding and subsequent measurements. This means that the first and last measurement cycles of each block cannot be used. Since in our study blocks were composed of 10 cycles, applying eq. 5

without modification would result in exclusion of 20% of the data, resulting in some loss of precision. To get around this problem, the average slope of each block was used to estimate the corrections for the first and last cycles. This approximation is justified by the fact that signal changes were nearly linear over the duration of each individual block.

As shown in Table 4, applying the decay time correction changes the final calculated $^{186}\text{Os}/^{188}\text{Os}$ ratio by -8 to +72 ppm, with an average change of +19 ppm. However, the overall range of variation of $^{186}\text{Os}/^{188}\text{Os}$ values is essentially unaffected (change of 2 ppm), indicated that this correction has not improved the reproducibility. This is probably because the slopes of the signal changes were similar (slowly decreasing) for most runs, leading to similar decay time corrections, and because application of equation 5 may have added some noise due to small random signal variations between cycles used to calculate the instantaneous slopes. Nevertheless, even though the decay time correction does not improve the reproducibility, it should improve the accuracy of the result as it takes into account the physical behavior of the amplifiers.

Isobaric interferences

The isotope ^{186}W is a direct isobaric interference on ^{186}Os . As noted above, the size of this interference is estimated by measuring the mass 231 peak by ion counting before and after each run or run segment, and subtracting for the heavy oxides of PtO_2 (Luguet et al., 2008), which are themselves estimated by measuring masses 228 ($^{196}\text{PtO}_2$) and 230 ($^{198}\text{PtO}_2$). Assuming that no other interfering species are present, this yields the intensity of $^{183}\text{WO}_3$ in counts per second (cps), which is multiplied by the natural $^{186}\text{W}/^{183}\text{W}$ ratio and the cps to V conversion factor to obtain the isobaric interference of $^{186}\text{WO}_3$ on $^{186}\text{OsO}_3$. Analogous procedures are used to calculate the isobaric interference of $^{187}\text{ReO}_3$ on $^{187}\text{OsO}_3$.

In most cases, fewer than 5 cps of $^{183}\text{WO}_3$ were present, leading to calculated corrections to $^{186}\text{Os}/^{188}\text{Os}$ of less than 0.000006 (3 to 48 ppm with an average of 24 ppm; Table 4). In a few cases, however, the corrections were considerably larger, either because the PtO_2 -corrected mass 231 peak was higher (up to 16 cps, analysis 19) or because the OsO_3 intensity was quite low (e.g., analysis 22). More disturbingly, these corrections do not seem to fully account for the entire budget of interferences isobaric with $^{186}\text{OsO}_3$. As seen in Fig. 4, even after correction the analyses with large calculated interferences (effect on $^{186}\text{Os}/^{188}\text{Os} > 0.000010$) have $^{186}\text{Os}/^{188}\text{Os}$ ratios that plot substantially above the range defined by the analyses with smaller interferences.

Two non-exclusive hypotheses can be proposed to explain why the measured interferences do not seem to adequately account for the interferences present on the $^{186}\text{OsO}_3$ peak. One is that molecular interferences other than $^{186}\text{WO}_3$ may be present. This possibility has been raised by previous authors, such as Chatterjee and Lassiter (2015) who suggest organic molecules as a possible isobaric contaminant. Interferences on mass 233 that cannot be fully explained by $^{185}\text{ReO}_3$ are frequently observed in $^{187}\text{Os}/^{188}\text{Os}$ studies, suggesting that species other than oxides of W, Re, Pt and Os may be present in the mass range of interest. Though there is not a perfect correlation, the fact that the interference corrections yield unsatisfactory results when the mass 231 peak is large suggest that unidentified molecular species in addition to $^{183}\text{WO}_3$ sometimes fall on this mass. Yin et al. (1993) suggested that certain Ba-bearing species ($^{138}\text{Ba}^{16}\text{OHBr}^-$ and $^{138}\text{Ba}^{16}\text{O}_6^-$) isobaric with $^{186}\text{OsO}_3^-$ may be present in NTIMS analyses. This suggestion is plausible, as the DROsS standard used for our study is dissolved in HBr, and Ba is an integral constituent of the loading solution. In the scan shown in Fig. 10, masses 222, 223 and 225 are present in the relative abundances of ^{134}Ba , ^{135}Ba and ^{137}Ba , with possible ^{136}Ba and ^{138}Ba -bearing species hidden by the large PtO_2 peaks, arguing for the existence of Ba compounds not far from the mass range of interest. If the BaOHBr^- and/or BaO_6^- species suggested by Yin et al. are indeed present, ^{138}Ba bearing molecules on mass 234 would be associated with ~ 11 times less abundant ^{135}Ba bearing molecules on mass 231. Considering mass 231 to be composed solely of $^{183}\text{WO}_3$ would then lead to undercorrection of the interference. Potentially significant molecular interferences are listed in Table 5.

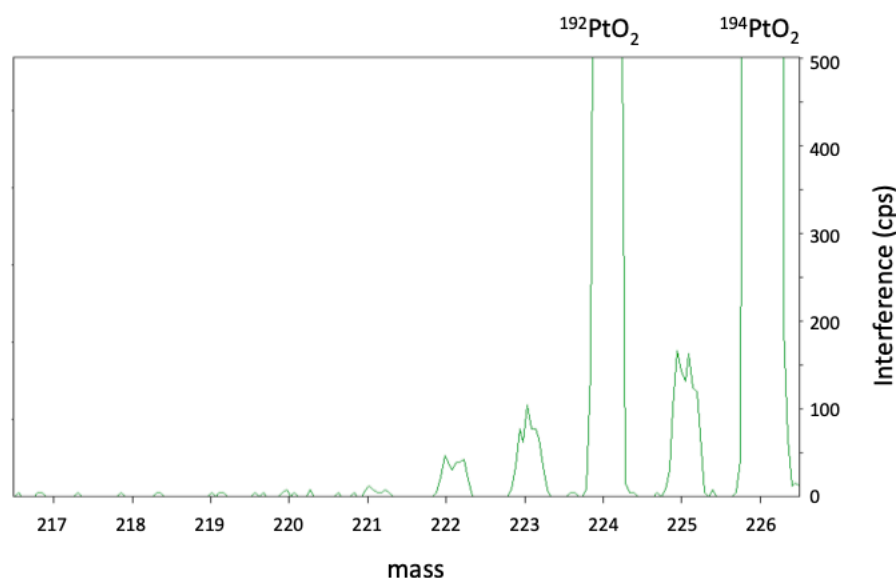


Figure 10. SEM scan in the mass range of 217 to 226. In addition to the two large PtO_2 peaks, three small but non-negligible peaks are observed, indicating that unidentified molecular ion beams exist close to the range of interest. These peaks have the relative abundances of ^{134}Ba , ^{135}Ba , and ^{137}Ba , suggesting that they may be Ba-bearing species. The search for such peaks closer to mass 234 ($^{186}\text{OsO}_3$) is complicated by the presence of PtO_2 , WO_3 and ReO_3 peaks.

Mass:	228	229	230	231	232	233	234	235	236
Main Os species:					$^{184}\text{Os}^{16}\text{O}_3$		$^{186}\text{Os}^{16}\text{O}_3$	$^{187}\text{Os}^{16}\text{O}_3$	$^{188}\text{Os}^{16}\text{O}_3$
	$^{194}\text{Pt}^{16}\text{O}^{18}\text{O}$ $^{195}\text{Pt}^{16}\text{O}^{17}\text{O}$ $^{196}\text{Pt}^{16}\text{O}_2$		$^{182}\text{W}^{16}\text{O}_3$	$^{183}\text{W}^{16}\text{O}_3$	$^{184}\text{W}^{16}\text{O}_3$	$^{185}\text{Re}^{16}\text{O}_3$	$^{186}\text{W}^{16}\text{O}_3$		
			$^{194}\text{Pt}^{18}\text{O}_2$ $^{196}\text{Pt}^{16}\text{O}^{18}\text{O}$ $^{198}\text{Pt}^{16}\text{O}_2$	$^{195}\text{Pt}^{18}\text{O}_2$ $^{198}\text{Pt}^{16}\text{O}^{17}\text{O}$	$^{196}\text{Pt}^{18}\text{O}_2$ $^{198}\text{Pt}^{16}\text{O}^{18}\text{O}$		$^{198}\text{Pt}^{18}\text{O}_2$		
			$^{134}\text{Ba}^{16}\text{OH}^{79}\text{Br}$ $^{134}\text{Ba}^{16}\text{O}_6$	$^{135}\text{Ba}^{16}\text{OH}^{79}\text{Br}$ $^{135}\text{Ba}^{16}\text{O}_6$	$^{134}\text{Ba}^{16}\text{OH}^{81}\text{Br}$ $^{136}\text{Ba}^{16}\text{OH}^{79}\text{Br}$ $^{136}\text{Ba}^{16}\text{O}_6$	$^{135}\text{Ba}^{16}\text{OH}^{81}\text{Br}$ $^{137}\text{Ba}^{16}\text{OH}^{79}\text{Br}$ $^{137}\text{Ba}^{16}\text{O}_6$	$^{136}\text{Ba}^{16}\text{OH}^{81}\text{Br}$ $^{138}\text{Ba}^{16}\text{OH}^{79}\text{Br}$ $^{138}\text{Ba}^{16}\text{O}_6$	$^{137}\text{Ba}^{16}\text{OH}^{81}\text{Br}$	$^{138}\text{Ba}^{16}\text{OH}^{81}\text{Br}$

Table 5. Potential molecular isobaric interferences on the masses of interest discussed in the text. Minor interferences involving higher order terms are ignored. A more complete table of possible interferences including masses up to 246 can be found in Luguët et al. (2007).

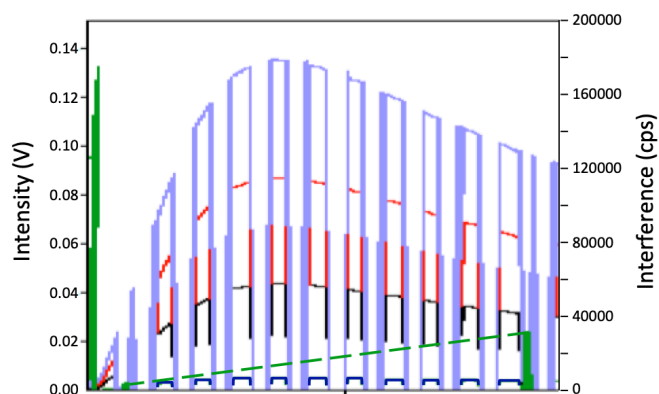
A second potential explanation for the poor performance of the interference correction when the measured interferences are large is that the interpolation procedure may not adequately account for the level of interferences present during data collection. This effect could pose problems even if all of the isobarically interfering species are correctly identified. Fig. 11A shows the first run of analysis 26. It is evident that simple linear interpolation between the interferences measured before and after this run is unlikely to provide accurate estimates of the interferences present during each acquisition cycle. A further complication arises from the fact that potential interferences and the OsO_3 signal do not vary synchronously (Fig. 11B). This problem can be partially addressed by interspersing short data collection runs with interference measurements (as was done in the example of analysis 28, shown in Fig. 11B), so that interpolated values more closely approximate the actual interferences present at the time of data acquisition. In contrast, analysis 24 (Fig. 11C) provides an example of an action to avoid. In this analysis, which consisted of a single run, the temperature of the filament was increased between each block to compensate for the rapidly dying signal. It is clear that linear interpolation of the interferences measured before and after this run will not accurately approximate the interferences present at the times of data acquisition, which may explain why the calculated $^{186}\text{Os}/^{188}\text{Os}$ ratio of this analysis is rather high (0.1199465), though within error of the average value. We suggest that if it is necessary to change the filament temperature during a run interference peaks should be measured before and after doing so.

As indicated in Table 4, interferences were considerably larger when analyses were performed using single Pt filaments (session 3) rather than double Pt filaments (sessions 1 and 2). In the double filament configuration the same current was applied to both filaments. Higher filament currents, typically by about 0.05 to 0.1 amps, were required for single filaments relative to double filaments to achieve similar levels of OsO_3^- emission and ionization. This may be because in the double filament configuration, radiative heating from the ionization filament helps to heat the sample loaded on the evaporation filament, allowing emission at lower current levels. We note that the source of the instrument was baked prior to analytical session 3, arguing that the interferences were derived from the filament material rather than from pollution in the source. We tentatively suggest that the lower current levels required in the double filament case may have limited the release of impurities from the filament material. Though further testing is needed, use of a double rather than a single filament configuration seems advisable.

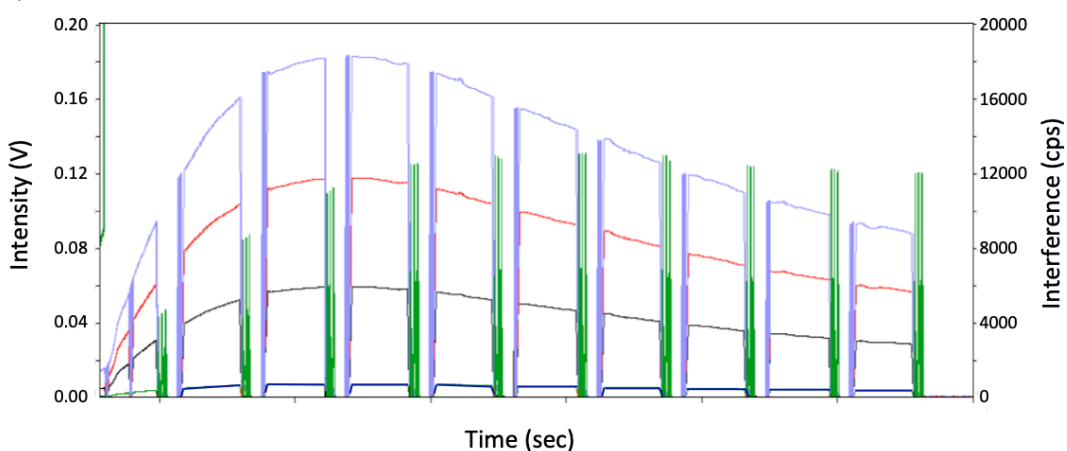
We conclude that there is still room for improvement when addressing the issue of interference corrections on small $^{186}\text{OsO}_3^-$ signals measured with 10^{13} Ohm amplifiers. All of the samples

defined as "good" in Table 4 had calculated corrections for $^{186}\text{WO}_3^-$ on the $^{186}\text{Os}/^{188}\text{Os}$ ratio < 0.0000060 , and their average $^{186}\text{Os}/^{188}\text{Os}$ value agrees within uncertainty with those of previous studies. Nevertheless, the fact that unsatisfactory results are obtained for calculated interference corrections on $^{186}\text{Os}/^{188}\text{Os} > 0.0000100$ implies that there may be smaller effects on analyses with only minor corrections, but that the resulting errors are too small to be recognized at the current uncertainty level. In this case the average $^{186}\text{Os}/^{188}\text{Os}$ ratio obtained in our study could be slightly too high (Fig. 4B). While the precisions of the individual low-interference analyses (indicated as "1" in Table 2) are similar to those expected from J-N noise and counting statistics (Fig. 5A), the overall reproducibility of these analyses (85 ppm) may not be optimal, as discussed above. Imperfect interference correction is one potential explanation for this somewhat higher than expected variability between analyses. Finally, we stress that the potential issues related to interferences discussed here are a consequence of the measurement of very small signals and do not in any way reflect a flaw in the 10^{13} Ohm amplifiers.

A)



B)



C)

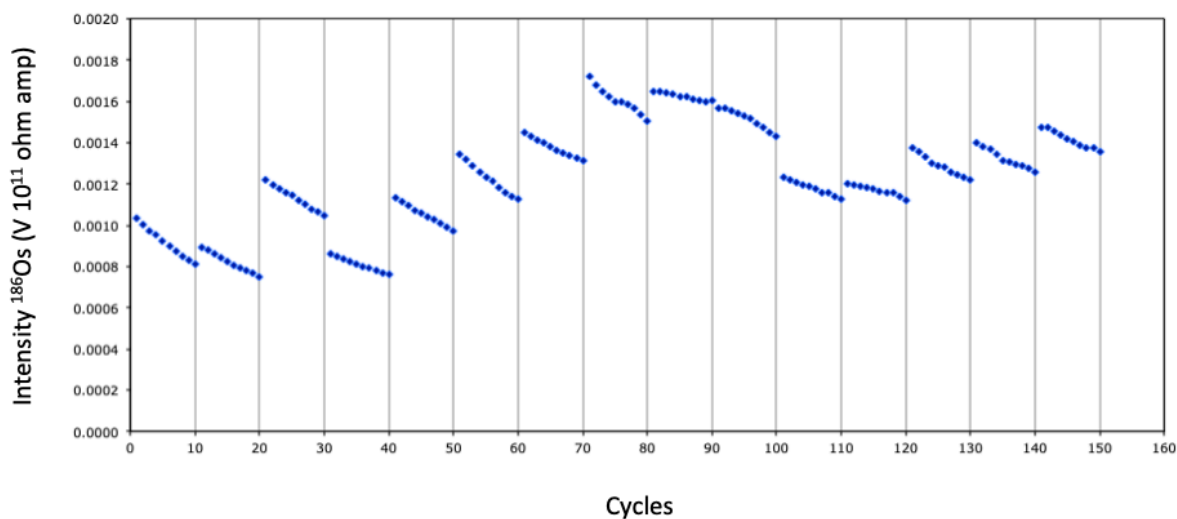


Figure 11. A) First run of analysis 26. Linear interpolation of interferences (green) measured before and after run would not accurately approximate interference levels during data acquisition. violet: $^{192}\text{OsO}_3$; red: $^{190}\text{OsO}_3$; black: $^{188}\text{OsO}_3$; dark blue: $^{186}\text{OsO}_3$. Interference runs were composed of 3 cycles of SEM measurements of masses 228 ($^{196}\text{PtO}_2$); 230 ($^{198}\text{PtO}_2$); 231 ($^{183}\text{WO}_3$); 232 ($^{184}\text{OsO}_3$); 233 ($^{185}\text{ReO}_3$). B) Analysis 28, included nine data acquisition runs each preceded and succeeded by interference runs, programmed in the sequence routine. Signals and interferences do not evolve at the same rates, but interpolation of frequent interference measurements can nevertheless allow for acceptable correction of known interferences. Colors as in (A). C) Evolution of the $^{186}\text{OsO}_3$ signal in run 1 of analysis 24. Filament was heated before each 10 cycle block to keep signal at an acceptable level. Interpolation of interferences taken before and after the 15 block run would be unlikely to produce reliable corrections.

Heavy oxide corrections

It has long been recognized that variations in the oxygen isotopic composition in the ion source and/or in the BaOH loading solution could significantly influence the calculated $^{186}\text{Os}/^{188}\text{Os}$ ratio in NTIMS measurements. To address this problem, authors have determined the ^{18}O and ^{17}O abundances in their instruments by a variety of methods, including dedicated analyses of large beams of ReO_4 (Brandon et al., 2006; Luguét et al., 2008), long term monitoring of periodically determined values (Ireland et al., 2011), pre- and post-run measurements (Chatterjee and Lassiter, 2015), and in-run cycle by cycle heavy oxide measurements during Os analyses (Chu et al., 2015; Luguét et al., 2008). These studies have generally concluded that oxygen isotope variations have a small, but not completely negligible, effect on the calculated $^{186}\text{Os}/^{188}\text{Os}$ composition. To evaluate the extent to which this effect might influence the much smaller signals measured with the 10^{13} Ohm amplifiers we used one of these amplifiers to measure mass 242, which is essentially composed of $^{192}\text{Os}^{16}\text{O}_2^{18}\text{O}^-$, simultaneously with the measurement of the main OsO_3^- peaks. After subtracting calculated expected abundances of rare OsO_3 isotopologues containing two or three heavy oxygen atoms from masses 240 and 242, the mass(242)/mass(240) ratio was used to calculate the $^{18}\text{O}/^{16}\text{O}$ ratio in the ion source. The oxygen terrestrial fractionation line (TFL) was then used to determine the corresponding $^{17}\text{O}/^{16}\text{Os}$ ratio, assuming that the TFL passes through the composition of Vienna Standard Mean Ocean Water (VSMOW). The $^{18}\text{O}/^{16}\text{O}$ ratios obtained from the analyses are shown in Table 2, and yield an average value of 0.0020179 ± 0.0000119 (2σ), which corresponds to a $^{17}\text{O}/^{16}\text{O}$ value of 0.0003812 ± 0.0000012 . These results are compared to values obtained in other laboratories in Fig. 12. The in-run 2SE uncertainties on the measured $^{18}\text{O}/^{16}\text{O}$ ratios of each analysis are nearly all much smaller than the range of the mean values of all analyses, suggesting that there is very limited oxygen isotope fractionation during analyses, but more substantial fractionation between analyses.

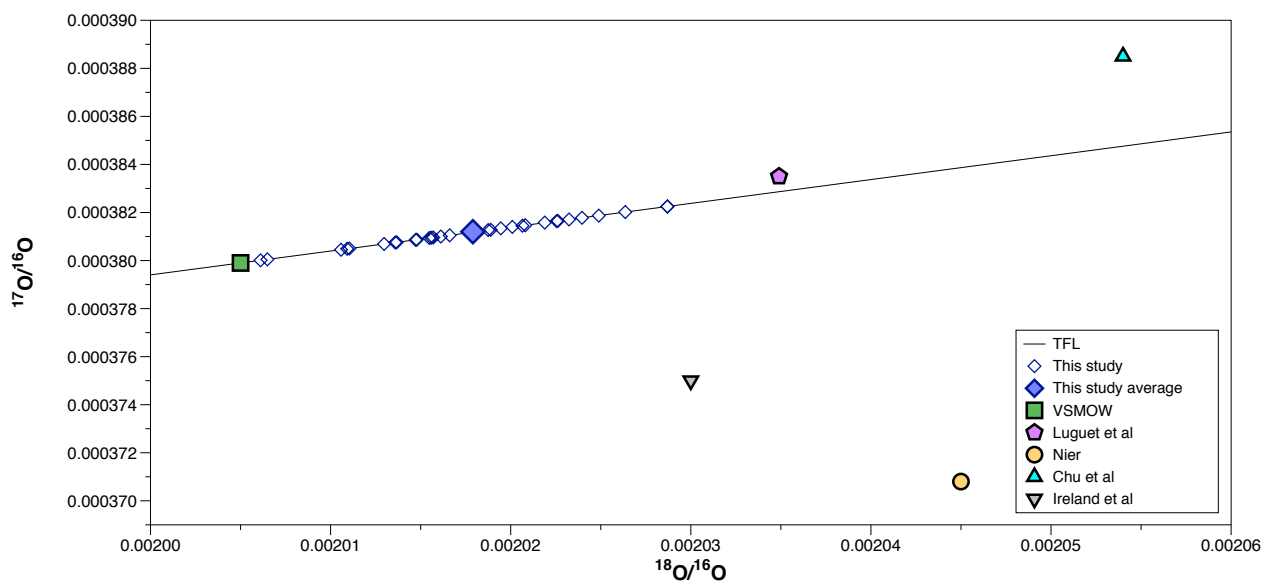


Figure 12. $^{18}\text{O}/^{16}\text{O}$ ratios measured in-run on the CRPG Triton mass spectrometer. The $^{17}\text{O}/^{16}\text{O}$ s compositions are estimated from the measured $^{18}\text{O}/^{16}\text{O}$ s ratios by assuming that all analyses should plot on the Terrestrial Fractionation Line (TFL) passing through the VSMOW value. Literature values are shown for comparison.

For all analyses, the effect of the heavy oxide contributions on the $^{186}\text{Os}/^{188}\text{Os}$ ratios was corrected using the measured in-run oxygen isotope composition, and compared with the $^{186}\text{Os}/^{188}\text{Os}$ ratio obtained assuming a fixed oxygen composition. For the latter we used the values ($^{18}\text{O}/^{16}\text{O} = 0.20349$; $^{17}\text{O}/^{16}\text{O} = 0.000380$) measured by Luguet et al. (2008) in a Triton mass spectrometer on ReO_4 . We chose to use this oxygen composition, rather than the classical values of Nier (1950), because it was measured in the same type of instrument and because it plots closer to the TFL. We found that the $^{186}\text{Os}/^{188}\text{Os}$ ratios obtained using the measured in-run oxygen compositions were 2 to 17 ppm higher (average 7 ppm) than those obtained using the fixed composition (Table 4). This very small but systematic shift would be removed if the average oxygen composition determined on our instrument were used for the fixed composition rather than that of Luguet et al. (2008). Use of the in-run measurements had essentially no effect (+1 ppm) on the overall variability of the thirty $^{186}\text{Os}/^{188}\text{Os}$ analyses. Thus it appears that variations in oxygen isotope composition have very little influence on the $^{186}\text{Os}/^{188}\text{Os}$ values measured on small signals with 10^{13} Ohm amplifiers.

Mass fractionation correction

The pioneering studies of $^{186}\text{Os}/^{188}\text{Os}$ variations (e.g. Brandon et al., 1999) used $^{189}\text{Os}/^{188}\text{Os}$ for mass bias correction as this ratio is less subject to perturbation by errors in oxygen composition than the more commonly used $^{192}\text{Os}/^{188}\text{Os}$ ratio. However, it became clear that uncertainties related to errors in oxygen isotope abundances are small compared to those induced by using a ratio with a small mass difference between numerator and denominator for this purpose. Thus $^{192}\text{Os}/^{188}\text{Os}$ is now usually employed for mass bias correction, and most authors (e.g. Brandon et al., 2007;

Chatterjee and Lassiter, 2015; Chu et al., 2015; Ireland et al., 2011; Luguet et al., 2008) adopt a normalizing value of 3.083, and assume that mass fractionation follows an exponential law. This facilitates comparison between studies, as contrasting mass bias correction procedures can induce differences in $^{186}\text{Os}/^{188}\text{Os}$ of several tens of ppm (see Chatterjee and Lassiter, 2015 and Luguet et al., 2008 for more complete discussions of this issue). One small difference concerns the study of Luguet et al. (2008), who added a second mass correction step to account for residual correlations between certain isotopic ratios observed after application of the normal mass fractionation procedure. This second correction lowers the $^{186}\text{Os}/^{188}\text{Os}$ ratio of the DROsS standard by about 20 ppm, likely explaining why the Luguet et al. value plots towards the bottom of the field in Fig. 4B.

We have adopted the standard mass bias correction procedures, which allow our data to be directly compared with earlier studies. As shown in Fig. 4B, our results agree within uncertainty with previous studies. Fig. 5A shows that the precisions on our analyses can be fully accounted for by J-N noise and counting statistics on the measured $^{186}\text{Os}/^{188}\text{Os}$ ratios. Thus any additional uncertainties introduced by the mass fractionation correction must be quite small. This is not unexpected. The relative J-N noise on the $^{192}\text{OsO}_3$ peak should be ~ 2.5 times smaller than that on the $^{186}\text{OsO}_3^-$ peak, because ^{192}Os is about 25 times more abundant than ^{186}Os , which more than compensates for the fact that $^{192}\text{OsO}_3^-$ is measured using a 10^{11} Ohm amplifier. Furthermore, any relative errors on the measured $^{192}\text{Os}/^{188}\text{Os}$ ratio will result in relative errors a factor of two smaller on the mass-fractionation corrected $^{186}\text{Os}/^{188}\text{Os}$ ratio. Taken together, this implies that uncertainties related to mass fractionation corrections are insignificant at current precision levels.

Conclusions and recommendations

This study shows that the theoretical limits of precision on $^{186}\text{Os}/^{188}\text{Os}$ ratios can be fully achieved on $^{186}\text{OsO}_3^-$ ion beams of 10 to 70 fA (0.001 to 0.007 V on a 10^{11} Ohm amplifier) measured with 10^{13} Ohm amplifiers. The long term reproducibility (2σ) obtained for signals in this range was 85 ppm, which approaches the reproducibility that can be theoretically expected ($2\sigma \sim 50$ to 80 ppm) for the range of counts of $^{186}\text{OsO}_3^-$ (1 to 3×10^9) and the signal intensities that encompass most of our analyses. The precision and reproducibility obtained here is sufficient to allow useful $^{186}\text{Os}/^{188}\text{Os}$ analyses of crustal rocks, which are expected to show much larger variations than mantle samples. As crustal rocks and sediments typically contain ~ 10 to 500 pg/g of Os, use of 10^{13} Ohm amplifiers would allow ^{186}Os data to be obtained from 10 to 500g of sample material, rather than the \sim kg quantities that are required for analyses using 10^{11} Ohm amplifiers. Nevertheless, if sufficient Os (typically tens of ng) is available to obtain large ($> \sim 800$ fA or 0.08 V) $^{186}\text{OsO}_3^-$ signals, use of 10^{11} Ohm amplifiers is preferable as these avoid the decay time issues discussed above, and allow the

possibility of multidynamic analyses. Similarly, 10^{12} Ohm amplifiers may be best adapted to $^{186}\text{OsO}_3^-$ signals in the range of ~ 100 to 800 fA. For $^{186}\text{OsO}_3^-$ ion beams greater than ~ 150 fA, signals for $^{188}\text{OsO}_3^-$, $^{189}\text{OsO}_3^-$, $^{190}\text{OsO}_3^-$, and $^{192}\text{OsO}_3^-$ will all approach or exceed the saturation limit for 10^{13} Ohm amplifiers (~ 1500 fA). The essential point is that the amplifier configuration should be chosen to fit the signal intensity.

We suggest here ways of optimizing the various aspects of $^{186}\text{Os}/^{188}\text{Os}$ NTIMS analyses of small samples with 10^{13} amplifiers, presented in order of decreasing importance.

Isobaric interferences. In this study, isobaric interferences were the largest single factor leading to inaccurate $^{186}\text{Os}/^{188}\text{Os}$ ratios. This is because the small signals that can be measured with the 10^{13} Ohm amplifiers are more sensitive to the presence of minor interferences than the much larger signals typically measured with 10^{11} Ohm amplifiers. Correction for these interferences is problematic when the calculated correction on $^{186}\text{Os}/^{188}\text{Os}$ is > 0.000100 . This is partly because molecular interferences on mass 234 may include species other than $^{186}\text{WO}_3$. Use of a double, rather than a single, Pt filament configuration seems to largely eliminate these unidentified interferences. Linear interpolation based solely on interference runs before and after the entire analysis does not adequately quantify potential $^{186}\text{WO}_3$ interferences because the interference and the OsO_3 signals do not vary synchronously, and neither species is likely to vary in a linear manner. Instead, it is recommended to measure interferences periodically throughout the analysis, allowing interpolation over shorter time periods, and to avoid heating between blocks.

Baselines. Johnson-Nyquist noise on the baseline is one of the most important sources of uncertainty. To minimize this effect, baselines should be measured for approximately the same amount of time as the signal itself. This can be done during slow heating before the analysis, as well as after data acquisition is terminated, to avoid sample waste and increase the sample yield. However, if this is done, short baselines should be performed several times during the analysis to monitor potential drift in the amplifiers.

Decay time corrections. If a mixed array of 10^{11} and 10^{13} amplifiers is used, it is important to apply a correction for their very different exponential decay times. In this study, this correction led to changes of -8 to $+72$ ppm in the final $^{186}\text{Os}/^{188}\text{Os}$ values, but did not improve the overall reproducibility. Nevertheless, this correction is based on the physical behavior of the amplifiers, thus its application should lead to final results that are more accurate.

Gain corrections. The gain calibration card used for detector arrays including both 10^{13} and 10^{11} Ohm amplifiers employs a 1.2 pA (120 mV) calibration current in negative ion mode, which is very far from full range of the 10^{11} Ohm amplifiers. As a result, the individual gain calibration values obtained for the 10^{11} Ohm amplifiers can vary by as much as 100 ppm from the average values. As the ^{192}Os peak used for the fractionation correction was measured on a 10^{11} Ohm amplifier, this occasionally led to spurious values. This problem can be alleviated by using the average gain factors obtained in the days preceding and following the measurement. Gain calibrations were normally performed during slow sample heating before each analysis. Using time-averaged gain values rather than individual readings improved the overall reproducibility of the $^{186}\text{Os}/^{188}\text{Os}$ by about 12 ppm, which is small but not completely negligible.

Oxide corrections. Variations in oxygen isotope composition had very little effect (several ppm) on the $^{186}\text{Os}/^{188}\text{Os}$ ratio in these measurements. It is quite simple to perform in-run oxygen composition determinations by measuring mass 242 ($^{192}\text{Os}^{16}\text{O}_2^{18}\text{O}$) with a 10^{13} Ohm amplifier to obtain $^{18}\text{O}/^{16}\text{O}$, and calculating $^{17}\text{O}/^{16}\text{O}$ from the terrestrial fractionation line. However, adequate results can also be obtained if the average oxygen isotope composition in the instrument is determined in separate measurements.

Acknowledgements

We thank Christiane Parmentier for technical assistance, Larry Shengold for helpful and animated discussions and Gareth Davies for an informal review. We also thank two anonymous reviewers for their constructive comments. This project was funded by the French ANR project INTOCC.

Data Availability Statement

The data that support the findings of this study are available from the corresponding author upon reasonable request.

References

- Brandon, A.D., Graham, D.W., Waight, T., Gautason, B., 2007. ^{186}Os and ^{187}Os enrichments and high- $3\text{He}/4\text{He}$ sources in the Earth's mantle: Evidence from Icelandic picrites. *Geochimica et Cosmochimica Acta* 71, 4570–4591. <https://doi.org/10.1016/j.gca.2007.07.015>
- Brandon, A.D., Norman, M.D., Walker, R.J., Morgan, J.W., 1999. ^{186}Os - ^{187}Os systematics of Hawaiian picrites. *Earth Planet. Sci. Lett.* 174, 25–42.

- Brandon, A.D., Snow, J.E., Walker, R.J., Morgan, J.W., Mock, T.D., 2000. ^{190}Pt - ^{186}Os and ^{187}Re - ^{187}Os systematics of abyssal peridotites. *Earth Planet. Sci. Lett.* 177, 319–335.
- Brandon, A.D., Walker, R.J., Puchtel, I.S., 2006. Platinum-osmium isotope evolution of the Earth's mantle: Constraints from chondrites and Os-rich alloys. *Geochim. Cosmochim. Acta* 70, 2093–2103.
- Chatterjee, R., Lassiter, J.C., 2016. $^{186}\text{Os}/^{188}\text{Os}$ variations in upper mantle peridotites: Constraints on the Pt/Os ratio of primitive upper mantle, and implications for late veneer accretion and mantle mixing timescales. *Chemical Geology* 442, 11–22. <https://doi.org/10.1016/j.chemgeo.2016.08.033>
- Chatterjee, R., Lassiter, J.C., 2015. High precision Os isotopic measurement using N-TIMS: Quantification of various sources of error in $^{186}\text{Os}/^{188}\text{Os}$ measurements. *Chemical Geology* 396, 112–123. <https://doi.org/10.1016/j.chemgeo.2014.12.014>
- Chu, Z.-Y., Li, C.-F., Chen, Z., Xu, J.-J., Di, Y.-K., Guo, J.-H., 2015. High-Precision Measurement of $^{186}\text{Os}/^{188}\text{Os}$ and $^{187}\text{Os}/^{188}\text{Os}$: Isobaric Oxide Corrections with In-Run Measured Oxygen Isotope Ratios. *Anal. Chem.* 87, 8765–8771. <https://doi.org/10.1021/acs.analchem.5b01689>
- Craig, G., Hu, Z., Zhang, A., Lloyd, N.S., Bouman, C., Schwieters, J., 2017. Dynamic time correction for high precision isotope ratio measurements.
- Creaser, R.A., Papanastassiou, D., Wasserburg, G.J., 1991. Negative thermal ion mass spectrometry of osmium, rhenium, and iridium. *Geochim. Cosmochim. Acta* 55, 397–401.
- Creech, J.B., Schaefer, B.F., Turner, S.P., 2020. Application of 10(13) omega Amplifiers in Low-Signal Plasma-Source Isotope Ratio Measurements by MC-ICP-MS: A Case Study with Pt Isotopes. *Geostand. Geoanal. Res.* 44, 223–229. <https://doi.org/10.1111/ggr.12310>
- Day, J.M.D., O'Driscoll, B., 2019. Ancient high Pt/Os crustal contaminants can explain radiogenic ^{186}Os in some intraplate magmas. *Earth and Planetary Science Letters* 519, 101–108. <https://doi.org/10.1016/j.epsl.2019.04.039>
- Ireland, T.J., Walker, R.J., Brandon, A.D., 2011. Os- ^{186}Os - ^{187}Os systematics of Hawaiian picrites revisited: New insights into Os isotopic variations in ocean island basalts. *Geochim. Cosmochim. Acta* 75, 4456–4475. <https://doi.org/10.1016/j.gca.2011.05.015>
- Johnson, J.B., 1928. Thermal Agitation of Electricity in Conductors. *Phys. Rev.* 32, 97–109. <https://doi.org/10.1103/PhysRev.32.97>
- Kimura, J.-I., Chang, Q., Kanazawa, N., Sasaki, S., Vaglarov, B.S., 2016. High-precision in situ analysis of Pb isotopes in glasses using 1013 Ω resistor high gain amplifiers with ultraviolet femtosecond laser ablation multiple Faraday collector inductively coupled plasma mass spectrometry. *J. Anal. At. Spectrom.* 31, 790–800. <https://doi.org/10.1039/C5JA00374A>
- Klaver, M., Smeets, R.J., Koornneef, J.M., Davies, G.R., Vroon, P.Z., 2015. Pb isotope analysis of ng size samples by TIMS equipped with a 1013 Ω resistor using a ^{207}Pb - ^{204}Pb double spike. *J. Anal. At. Spectrom.* 31, 171–178. <https://doi.org/10.1039/C5JA00130G>
- Koornneef, J.M., Bouman, C., Schwieters, J.B., Davies, G.R., 2014. Measurement of small ion beams by thermal ionisation mass spectrometry using new 1013Ohm resistors. *Analytica Chimica Acta* 819, 49–55. <https://doi.org/10.1016/j.aca.2014.02.007>
- Liu, J., Pearson, D.G., 2014. Rapid, precise and accurate Os isotope ratio measurements of nanogram to sub-nanogram amounts using multiple Faraday collectors and amplifiers equipped with 1012 Ω resistors by N-TIMS. *Chemical Geology* 363, 301–311. <https://doi.org/10.1016/j.chemgeo.2013.11.008>
- Luguet, A., Nowell, G.M., Pearson, D.G., 2008. $^{184}\text{Os}/^{188}\text{Os}$ and $^{186}\text{Os}/^{188}\text{Os}$ measurements by negative thermal ionisation mass spectrometry (NTIMS): Effects of interfering element and mass fractionation corrections on data accuracy and precision. *Chem. Geol.* 248 (special issue HSE Geochemistry), 342–362.
- McDaniel, D.K., Walker, R.J., Hemming, S.R., Horan, M.F., Becker, H., Grauch, R.I., 2004. Sources of osmium to the modern oceans: new evidence from the ^{190}Pt - ^{186}Os system | Associate editor: E. M. Ripley. *Geochimica et Cosmochimica Acta* 68, 1243–1252. <https://doi.org/10.1016/j.gca.2003.08.020>
- Nier, A.O., 1950. A Redetermination of the Relative Abundances of the Isotopes of Carbon, Nitrogen, Oxygen, Argon, and Potassium. *Phys. Rev.* 77, 789–793. <https://doi.org/10.1103/PhysRev.77.789>

- Nyquist, H., 1928. Thermal Agitation of Electric Charge in Conductors. *Phys. Rev.* 32, 110–113. <https://doi.org/10.1103/PhysRev.32.110>
- Puchtel, I.S., Brandon, A.D., Humayun, M., 2004. Precise Pt–Re–Os isotope systematics of the mantle from 2.7-Ga komatiites. *Earth and Planetary Science Letters* 224, 157–174. <https://doi.org/10.1016/j.epsl.2004.04.035>
- Quadt, A. von, Wotzlaw, J.-F., Buret, Y., Large, S.J.E., Peytcheva, I., Trinquier, A., 2016. High-precision zircon U/Pb geochronology by ID-TIMS using new 1013 ohm resistors. *J. Anal. At. Spectrom.* 31, 658–665. <https://doi.org/10.1039/C5JA00457H>
- Trinquier, A., Komander, P., 2016. Precise and accurate uranium isotope analysis by modified total evaporation using 10(13) ohm current amplifiers. *J. Radioanal. Nucl. Chem.* 307, 1927–1932. <https://doi.org/10.1007/s10967-015-4400-2>
- Volkening, J., Walczyk, T., Heumann, K.G., 1991. Osmium isotope determinations by negative thermal ionization mass spectrometry. *Int. J. Mass Spec. Ion Phys.* 105, 147–159.
- Walker, R.J., Morgan, J.W., Beary, E.S., Smoliar, M.I., Czamanske, G.K., Horan, M.F., 1997. Applications of the 190Pt-186Os isotope system to geochemistry and cosmochemistry. *Geochim. Cosmochim. Acta* 61, 4799–4807.
- Wang, G., Vollstaedt, H., Xu, J., Liu, W., 2019. High-Precision Measurement of 187Os/188Os Isotope Ratios of Nanogram to Picogram Amounts of Os in Geological Samples by N-TIMS using Faraday Cups Equipped with 1013 Ω Amplifiers. *Geostandards and Geoanalytical Research* 43, 419–433. <https://doi.org/10.1111/ggr.12269>
- Yin, Q.Z., Jagoutz, E., Verkhovskiy, A.B., Wänke, H., 1993. 187Os-186Os and 187Os-188Os method of dating: An introduction. *Geochimica et Cosmochimica Acta* 57, 4119–4128. [https://doi.org/10.1016/0016-7037\(93\)90358-4](https://doi.org/10.1016/0016-7037(93)90358-4)